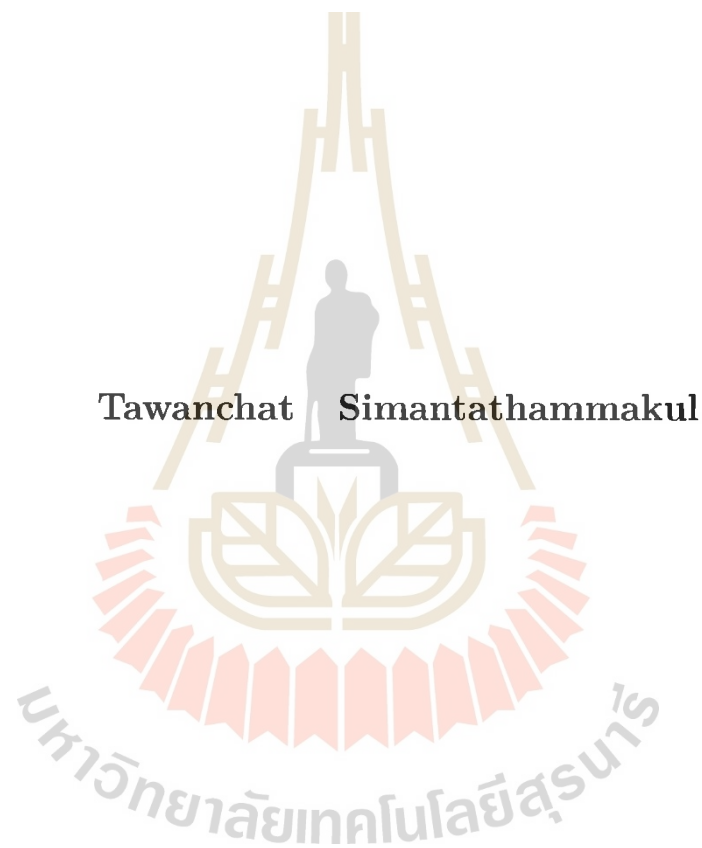


**ANALYSIS OF CHARMONIUM PRODUCTION  
IN  $pp$  COLLISIONS AT  $\sqrt{s} = 13$  TeV WITH  
ALICE AT THE LHC**



**Tawanchat Simantathammakul**

**A Thesis Submitted in Partial Fulfillment of the Requirements for the  
Degree of Master of Science in Physics  
Suranaree University of Technology  
Academic Year 2019**

การวิเคราะห์การผลิตอนุภาคชาร์มโมเนียมในการชนกันของอนุภาคโปรตอนที่  
มีพลังงานสิบสามเทระอิเล็กตรอนโวลต์ โดยเครื่องตรวจจับอนุภาคดิซ ณ  
เครื่องเร่งอนุภาคขนาดใหญ่ แอลเอชซี



นายตะวันฉัตร สิ้นตธรรมกุล

วิทยานิพนธ์นี้เป็นส่วนหนึ่งของการศึกษาตามหลักสูตรปริญญาวิทยาศาสตรมหาบัณฑิต  
สาขาวิชาฟิสิกส์  
มหาวิทยาลัยเทคโนโลยีสุรนารี  
ปีการศึกษา 2562

**ANALYSIS OF CHARMONIUM PRODUCTION IN  $pp$   
COLLISIONS AT  $\sqrt{s} = 13$  TeV WITH ALICE AT THE LHC**

Suranaree University of Technology has approved this thesis submitted in partial fulfillment of the requirements for a Master degree.

Thesis Examining Committee



(Assoc. Prof. Dr. Panomsak Meemon)

Chairperson



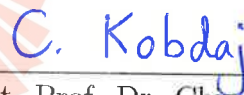
(Asst. Prof. Dr. Christoph Herold)

Member (Thesis Advisor)



(Prof. Dr. Yupeng Yan)

Member



(Asst. Prof. Dr. Chinorat Kobdaj)

Member



(Dr. Benjamin Dönigus)

Member



(Assoc. Prof. Flt. Lt. Dr. Kontorn Chamniprasart)

Vice Rector for Academic Affairs  
and Internationalization



(Assoc. Prof. Dr. Worawat Meevasana)

Dean of Institute of Science

ตระวันฉัตร สีมันตรธรรมกุล : การวิเคราะห์การผลิตอนุภาคชาร์มโมเนียมในการชนกันของ  
อนุภาคโปรตอนที่มีพลังงานสิบสามเทระอิเล็กตรอนโวลต์โดยเครื่องตรวจจับอนุภาคอลิซ  
ณ เครื่องเร่งอนุภาคขนาดใหญ่ แอลเอชซี (ANALYSIS OF CHARMONIUM  
PRODUCTION IN  $pp$  COLLISIONS AT  $\sqrt{s} = 13$  TeV WITH ALICE AT THE LHC)  
อาจารย์ที่ปรึกษา : ผู้ช่วยศาสตราจารย์ ดร.คริสทอฟ เฮโรลด์, 60 หน้า .

ผู้วิจัยต้องการวิเคราะห์การสลายตัวเป็นอนุภาคแฮดรอนของ  $\eta_c J/\psi \rightarrow p\bar{p}$  ในการชนกัน  
ของอนุภาคโปรตอนที่มีพลังงานสิบสามเทระอิเล็กตรอนโวลต์ด้วยเครื่องตรวจจับอนุภาคอลิซ ณ  
เครื่องเร่งอนุภาคขนาดใหญ่ แอลเอชซี ซึ่งข้อมูลนำมาจาก AliEn (ALICE Environment Grid  
Framework) โดยใช้ซอฟต์แวร์ AliRoot และ AliPhysics ทั้งนี้ เพื่อที่จะค้นหาอนุภาคที่มีช่วงชีวิตสั้น  
การจำลองมวลคงที่ คือวิธีในการจัดหาอนุภาคที่ถูกเลือกจากการสำรวจ ได้จากการรวมกันของ  
อนุภาคที่ได้จากการสลายตัว ซึ่งรวมถึงสัญญาณพื้นหลังที่ได้จากการรวมกันแม้ว่าจะไม่เกี่ยวข้อง  
และเพื่อจะลบสัญญาณพื้นหลังนี้ มีสามเทคนิคในการประมาณการกระจายตัวของสัญญาณพื้นหลัง  
ได้แก่ การจับคู่อนุภาคที่มีประจุเดียวกัน การผสมเหตุการณ์การชน และการหมุนเส้นทางการ  
เคลื่อนที่ของอนุภาค ซึ่งการผสมเหตุการณ์การชน และการหมุนเส้นทางการเคลื่อนที่ของอนุภาคให้  
ค่าตามสถิติเพียงพต่อการลบสัญญาณพื้นหลัง และจากผลลัพธ์ในปัจจุบันพบสัญญาณของอนุภาค  
 $\eta_c$  และ  $J/\psi$  ที่โมเมนตัมตามขวางในช่วง 6–8 GeV/c ด้วยมวลคงที่  $2.9625 \pm 0.0036$  GeV/c<sup>2</sup>  
และ  $3.0959 \pm 0.0018$  GeV/c<sup>2</sup> ตามลำดับ และมีนัยสำคัญของสัญญาณอยู่ที่ 3.7 และ 1.2 ตามลำดับ

สาขาวิชาฟิสิกส์  
ปีการศึกษา 2562

ลายมือชื่อนักศึกษา ศ. วิษณุ 30/06/2562  
ลายมือชื่ออาจารย์ที่ปรึกษา [ลายมือ]

TAWANCHAT SIMANTATHAMMAKUL : ANALYSIS OF  
CHARMONIUM PRODUCTION IN  $pp$  COLLISIONS AT  $\sqrt{s} = 13$  TeV  
WITH ALICE AT THE LHC. THESIS ADVISOR : ASST. PROF.  
CHRISTOPH HEROLD, Ph.D. 60 PP.

HIGH ENERGY PHYSICS/ALICE COLLABORATION/DATA ANALYSIS/  
CHARMONIUM

We analyze the hadronic decay of  $\eta_c, J/\psi \rightarrow p\bar{p}$  in proton-proton collisions at  $\sqrt{s} = 13$  TeV with ALICE at the LHC. The data are taken by the ALICE collaboration and stored through AliEn (ALICE Environment Grid Framework) using AliRoot and AliPhysics. To find these short-lived particles, the invariant mass reconstruction is the method to provide observed particle candidates from combinations of decay products, which includes uncorrelated combinatorial background. To subtract this background, there are three techniques to reproduce the shape of uncorrelated invariant mass, event mixing, like-sign pairs and track rotation. The event mixing and track rotation provide enough statistics for subtracting the background. The current results show the signal of  $\eta_c$  and  $J/\psi$  in the transverse momentum 6 - 8 GeV/c with the invariant mass  $2.9625 \pm 0.0035$  GeV/c<sup>2</sup> and  $3.0959 \pm 0.0018$  GeV/c<sup>2</sup>, respectively, with the significance 3.7 and 1.2, respectively.

School of Physics

Academic Year 2019

Student's Signature ทิวาฉัตร สิมานต์ถัมมากุล

Advisor's Signature Christoph Herold

# ACKNOWLEDGEMENTS

I would like to express my gratitude to the following people for their encouragement, assistance, and support which have enabled me to complete my thesis.

My deepest gratitude goes first and foremost to my thesis advisor Asst. Prof. Dr. Christoph Herold, Asst. Prof. Dr. Chinorat Kobdaj and to Dr. Benjamin Dönigus from Goethe University, Frankfurt, Germany for their support, patient guidance, consideration, and assistance throughout the study.

I would like to thank all lecturers in the School of Physics, who have taught me and made it possible to extend of my knowledge and my professional development in the past many academic years. Many thanks to our group members, nuclear and particle physics group, for valuable discussions and suggestions.

I would like to thank Assoc. Prof. Dr. Panomsak Meemon and Prof. Dr. Yupeng Yan for sitting at the thesis committee and giving me various excellent advices.

I also would like to thank Development and Promotion of Science and Technology Talents Project (DPST), Suranaree University of Technology (SUT), and National Science and Technology Development Agency (NASTDA) for funding and supporting to my research and thanks to A Large Ion Collider Experiment (ALICE) collaboration and Goethe-University Frankfurt am Main for allowing me to participate in international science projects.

Last but not least, I would like to extend my immense gratitude to my parents and my girlfriend, Patcharawee Munsaket for their continuous love, understanding, encouragement and support throughout the progress and for motivating me to complete my study.

Tawanchat Simantathammakul



# CONTENTS

	Page
ABSTRACT IN THAI . . . . .	I
ABSTRACT IN ENGLISH . . . . .	II
ACKNOWLEDGEMENTS . . . . .	III
CONTENTS . . . . .	V
LIST OF TABLES . . . . .	VIII
LIST OF FIGURES . . . . .	IX
LIST OF ABBREVIATIONS . . . . .	XIV
<b>CHAPTER</b>	
<b>I INTRODUCTION . . . . .</b>	<b>1</b>
<b>II CHARMONIUM . . . . .</b>	<b>3</b>
2.1 Heavy quarkonium . . . . .	3
2.2 Previous charmonium studies . . . . .	4
2.3 Charmonium production . . . . .	6
2.4 Decay modes . . . . .	6
<b>III THE ALICE EXPERIMENT . . . . .</b>	<b>8</b>
3.1 Large Hadron Collider (LHC) . . . . .	8
3.2 ALICE detector . . . . .	8
3.2.1 Inner Tracking System(ITS) . . . . .	10
3.2.2 Time Projection Chamber (TPC) . . . . .	12
3.2.3 Time of Flight Detector (TOF) . . . . .	12



## CONTENTS (Continued)

	<b>Page</b>
3.3 Detector performance . . . . .	13
3.3.1 Tracking . . . . .	13
3.3.2 Particle Identification (PID) . . . . .	14
3.4 ALICE analysis . . . . .	16
3.4.1 AliRoot/AliPhysics, the ALICE analysis framework . . . . .	16
<b>IV ANALYSIS OF CHARMONIUM DECAY TO PROTON- ANTIPROTON PAIR . . . . .</b>	<b>19</b>
4.1 Analysis Overview . . . . .	19
4.2 Retrieving data from ALICE GRID . . . . .	19
4.3 Event selection of $pp$ collision . . . . .	20
4.4 Proton and antiproton track selection . . . . .	21
4.4.1 Track quality requirements in ITS and TPC . . . . .	21
4.4.2 Particle identification selection . . . . .	22
4.5 Charmonium candidates selection using invariant mass reconstruc- tion . . . . .	28
4.6 Combinatorial Background Estimation . . . . .	30
4.6.1 Like-sign pair method . . . . .	32
4.6.2 Event-mixing method . . . . .	33
4.6.3 Track rotational method . . . . .	35
4.7 Background Subtraction . . . . .	37
4.8 Extraction of the signal . . . . .	41
4.9 Phase space simulation for two-body decays . . . . .	44
<b>V CONCLUSION . . . . .</b>	<b>47</b>

## CONTENTS (Continued)

	Page
REFERENCES . . . . .	50
APPENDIX . . . . .	55
CURRICULUM VITAE . . . . .	60



## LIST OF TABLES

Table		Page
2.1	List of charmed eta meson decay modes (Tanabashi et al., 2018).	7
2.2	List of charmonium states decaying into a proton-antiproton pair as final state (Tanabashi et al., 2018). . . . .	7
4.1	The $\eta_c$ and $J/\psi$ fit results from the candidate invariant mass spectra subtracting background by event mixing and track rotation methods. . . . .	43
1	The list of periods and good run numbers of proton-proton collisions with $\sqrt{s} = 13$ TeV in central barrel tracking in 2016. . . . .	57
2	The list of periods and number of runlists of proton-proton collisions with $\sqrt{s} = 13$ TeV in central barrel tracking in 2017. . . . .	58
3	The list of periods and number of runlists of proton-proton collisions with $\sqrt{s} = 13$ TeV in central barrel tracking in 2018. . . . .	59



# LIST OF FIGURES

Figure		Page
2.1	The diagram of the charmonium production from a B-meson decay (Teklishyn, 2014). . . . .	6
3.1	The schematic of the layout of the LHC including each of main experiments (Michel, 2020). . . . .	9
3.2	The schematic of ALICE detector (Tauro, 2017). . . . .	9
3.3	The schematic of ITS layers (The ALICE Collaboration et al., 2008). . . . .	10
3.4	Schematics of the Inner Tracking System during (a) Run 2 and (b) Run 3 (Tauro, 2017). . . . .	11
3.5	Schematic drawing of the ALICE TPC (Alme et al., 2010). . . . .	13
3.6	Event reconstruction flow in central barrel tracking (Alice Collaboration, 2014). . . . .	14
3.7	Specific energy loss ( $dE/dx$ ) versus particle momentum in the TPC in pp collisions at $\sqrt{s} = 13$ TeV. The lines show the parametrizations of the expected mean energy loss (ALICE collaboration, 2015). . . . .	15
3.8	TOF beta vs momentum performance plot in pp collisions at 13 TeV (ALICE collaboration, 2020). . . . .	16
3.9	The general schema of the AliRoot architecture (CERN Accelerating science, 2011). . . . .	17

## LIST OF FIGURES (Continued)

Figure		Page
4.1	Total $dE/dx$ spectrum versus TPC momentum in ALICE TPC from $pp$ collisions at $\sqrt{s} = 13$ TeV . . . . .	23
4.2	Total TOF speed ( $\beta$ ) versus TPC momentum in ALICE TOF from $pp$ collisions at $\sqrt{s} = 13$ TeV. . . . .	24
4.3	TOF mass of protons in ALICE TOF versus TPC momentum of protons in ALICE TPC. . . . .	24
4.4	TOF mass of antiprotons in ALICE TOF versus TPC momentum of antiprotons in ALICE TPC. . . . .	25
4.5	$n\sigma_{TPC}$ of proton's signals in ALICE TPC versus TPC momentum. . . . .	26
4.6	$n\sigma_{TOF}$ of proton's signals in ALICE TOF versus TPC momentum. . . . .	26
4.7	$n\sigma_{TPC}$ of proton and antiproton signal in ALICE TPC with the squared mass in the range between 0.7 - 1.1 $\text{GeV}^2/c^4$ versus TPC momentum. . . . .	27
4.8	$n\sigma_{TOF}$ of proton and antiproton signal in ALICE TOF with the squared mass in the range between 0.7 - 1.1 $\text{GeV}^2/c^4$ versus TPC momentum. . . . .	27
4.9	Total $dE/dx$ spectrum with the squared mass in the range between 0.7 - 1.1 $\text{GeV}^2/c^4$ versus TPC momentum in ALICE TPC from $pp$ collisions at $\sqrt{s} = 13$ TeV . . . . .	28
4.10	Total TOF speed ( $\beta$ ) versus with the squared mass in the range between 0.7 - 1.1 $\text{GeV}^2/c^4$ versus TPC momentum in ALICE TOF from $pp$ collisions at $\sqrt{s} = 13$ TeV. . . . .	29

## LIST OF FIGURES (Continued)

Figure		Page
4.11	The relation between $n\sigma_{TPC}$ and $n\sigma_{TOF}$ of proton/antiproton track that is measured by ALICE TPC and TOF from $pp$ collisions at $\sqrt{s} = 13$ TeV. . . . .	30
4.12	Total $dE/dx$ spectrum with the squared mass in the range between 0.7 - 1.1 $\text{GeV}^2/c^4$ , $ n\sigma_{TPC}  < 2$ , and $ n\sigma_{TOF}  < 5$ versus TPC momentum in ALICE TPC from $pp$ collisions at $\sqrt{s} = 13$ TeV . .	31
4.13	Total TOF speed ( $\beta$ ) versus with the squared mass in the range between 0.7 - 1.1 $\text{GeV}^2/c^4$ , $ n\sigma_{TPC}  < 2$ , and $ n\sigma_{TOF}  < 5$ versus TPC momentum in ALICE TOF from $pp$ collisions at $\sqrt{s} = 13$ TeV. . . . .	32
4.14	Kinematics of two-body decays and invariant mass reconstruction.	32
4.15	The invariant mass spectrum of charmonium candidates reconstructing from proton-antiproton pairs versus its transverse momentum in the midrapidity $ y  < 0.5$ . . . . .	33
4.16	Sketch two like-sign pairs reconstructing from two unlike-sign pairs.	34
4.17	The positive like-sign pairs of charmonium candidates reconstructing from proton-proton pairs versus its transverse momentum in the midrapidity $ y  < 0.5$ . . . . .	34
4.18	The negative like-sign pairs of charmonium candidates reconstructing from antiproton-antiproton pairs versus its transverse momentum in the midrapidity $ y  < 0.5$ . . . . .	35

## LIST OF FIGURES (Continued)

Figure		Page
4.19	Sketch of a mixed event pair by using positive charged particle from event 1 and negative charged particle from event 2. . . . .	36
4.20	The mixed event background of charmonium candidates reconstructing from proton-antiproton pairs versus its transverse momentum in the midrapidity $ y  < 0.5$ . . . . .	36
4.21	Sketch of the momentum vector of positive and negative track, where the positive track is rotated. After breaking the correlation, the reconstructed momentum of the mother do not point to the primary vertex. . . . .	37
4.22	The positive track rotational background of charmonium candidates reconstructing from rotated-proton and antiproton pairs versus its transverse momentum in the midrapidity $ y  < 0.5$ . . . . .	38
4.23	The negative track rotational background of charmonium candidates reconstructing from proton and rotated-antiproton pairs versus its transverse momentum in the midrapidity $ y  < 0.5$ . . . . .	39
4.24	Invariant mass spectrum of charmonium candidates with different integrated transverse momentum regions. . . . .	40
4.25	Invariant mass spectrum after subtraction of mixed event background with different integrated transverse momentum regions. . . . .	41
4.26	Invariant mass spectrum after subtraction of track rotational background with different integrated transverse momentum regions. . . . .	42
4.27	Invariant mass spectrum after subtraction of the mixed event background. . . . .	44

## LIST OF FIGURES (Continued)

Figure		Page
4.28	Invariant mass spectrum after subtraction of the track rotational background. . . . .	45
4.29	Invariant mass distribution of $\eta_c \rightarrow p\bar{p}$ candidates in the simulation of proton-proton collisions at $\sqrt{s}=13$ TeV. The top-left panel displays the invariant mass distribution of all unlike-sign pairs together with the background distribution estimated with the like-sign pair, event mixing, and track rotation methods. The top-left and both bottom panels show the invariant mass distribution with fit function after background subtraction from the like-sign pair, event mixing, track rotation method, respectively. . . . .	46



## LIST OF ABBREVIATIONS

ALEPH	Apparatus for Large Electron-positron PHysics
ALICE	A Large Ion Collider Experiment
AliEn	ALICE Environment Grid Framework
AliPhysics	ALICE Physics
AliRoot	ALICE Root
AOD	Analysis Object Data
DCA	Distance of Closest Approach
ESD	Event Summary Data
FLUKA	FLUktuierende KAskade
GEANT	GEometry ANd Tracking
GeV	Giga electron-Volts
HIJING	Heavy Ion Jet INteraction Generator
ITS	Inner Tracking System
LHC	Large Hadron Collider
ME	Mixed Event
MeV	Mega Electron-Volts
MRPCs	Multi-gap Resistive Plate Chambers
NRQCD	Non-Relativistic Quantum Chromo-Dynamics
PID	Particle Identification

**LIST OF ABBREVIATIONS (Continued)**

PWG	Physics Working Group
QCD	Quantum Chromo-Dynamics
QED	Quantum Electro-Dynamics
QGP	Quark-Gluon Plasma
SDD	Silicon Drift Detector
SE	Same Event
SPD	Silicon Pixel Detector
SSD	Silicon Strip Detector
TeV	Tera Electron-Volts
TOF	Time Of Flight
TPC	Time-Projection Chamber
SUT	Suranaree University of Technology

# CHAPTER I

## INTRODUCTION

In nature all elements are composed of atoms which are composed of sub-atomic particles, such as protons, neutrons, and electrons. Why protons and neutrons stick together in the nucleus, although their electric charges are positive and neutral, respectively?

In nuclear and particle physics, the smallest particle that they forms protons and neutrons is called “quark”. Quarks are elementary particles in the standard model which have never been found as isolated particle in nature because they are held together and confined by one of the four fundamental forces namely the strong interaction. In the standard model, there are six quark species and their six antiparticle, they are called “antiquarks”. The protons and the neutrons consist of two quark species and three quarks, “up” quark or u-quark and “down” quark or d-quark. Mass of u-quark is  $2.16 \text{ MeV}/c^2$ , electric charge is  $2/3e$  and the mass d-quark is  $4.67 \text{ MeV}/c^2$ , electric charge is  $-1/3e$  (Particle Data Group et al., 2020). so the masses of proton and neutron should be  $8.99$  and  $11.5 \text{ MeV}/c^2$ , respectively, but measurement show around  $938.272 \text{ MeV}/c^2$  for the proton and  $939.565 \text{ MeV}/c^2$  for the neutron. What causes the different masses and how can we study the relation between their masses and the strong nuclear interaction?

Charmonia as bound states of a charm-anticharm pairs provide an interesting opportunity for studying the strong interaction. While the initial quark-antiquark pair is produced in a hard-scattering process which can be described by

perturbative quantum chromodynamics, the quantum field theoretical formation of the string interaction in the standard model. The subsequent formation of the charmonium proceeds non-perturbatively and can be described in effective models (Voloshin, 2008). One of the objective of A Large Ion Collider Experiment (ALICE) (Alice Collaboration, 2014), performing one experiment at the Large Hadron Collider (LHC), is the study of charmonium in both proton-proton and nucleus-nucleus collisions, the latter on creating a quark-gluon plasma, which presumably influences the production and behavior of quarkonium states.

In this thesis, we focus on the production of two lowest-lying states of  $c\bar{c}$ , charmed eta meson ( $\eta_c$ ) and  $J/\psi$  in proton-proton collision at the top LHC beam energy of 13 TeV. Both of them can provide multitude of hadronic decay channels, whereas we choose the decay into a proton-antiproton pair final state that is currently being analyzed within the ALICE group.

The data produced by ALICE are stored in AliEn, The ALICE Environment Grid Framework. The data study have been done by using AliRoot, the analysis and simulation framework for ALICE, and AliPhysics to provide the analysis  $\sqrt{s} = 13$  TeV that are produced in 2016 until 2018.

The basic idea in the reconstruction of a certain decay channel is the determination of the invariant mass of the decay of products. Hereby, it is necessary to identify those particles, in our case proton-antiproton pairs, that stem from the decay of  $\eta_c$  meson and  $J/\psi$ , and separate them from other random pairs of protons and antiprotons which are produced by other sources, the so-called combinatorial background.

# CHAPTER II

## CHARMONIUM

### 2.1 Heavy quarkonium

Quarkonium is a composite of a heavy quark and its own antiquark. It is the simplest system to probe such kind of physics. Two quarkonium systems, charmonium  $c\bar{c}$  and bottomonium  $b\bar{b}$  are used for quantum chromodynamics (QCD) studies. The strong force provides the interaction between quarks, mediated by gluons, confining them together in hadrons, described by QCD. Quarks exist in three different colour states, denoted as red, green and blue. The colour charge of quarks and gluons in strong interactions is a quantum number similar to the hypercharge and weak isospin projection in electroweak interactions.

The model to describe the bound  $c\bar{c}$  state is non-relativistic QCD (NRQCD). Quarks are bound by strong force with a gluon as a exchange particle. Since gluon and photon are massless vector particles, so the QCD is similar to quantum electrodynamics (QED) for small  $r$ . The potential of single gluon exchange is Coulomb-like interaction 2.1. At the large distance, both quarks are confined. Thus, the potential increase without limit which is represented by distance-independent potential.

$$V(r) = -\frac{4}{3} \frac{\alpha_s}{r} + br, \quad (2.1)$$

where  $\alpha_s$  is strong coupling constant and  $b$  is string tension. Due to the fact that mass of heavy quark is very large, the system is non-relativistic, quarkonium

can be described in terms of the heavy quark bound state velocity,  $v \ll 1$ , and by the energy scales. The strong coupling constant can be written as the function of interaction energy( $Q$ ) and approximated by

$$\alpha_s(Q^2) \approx \frac{12\pi}{(33 - 2n_f)\ln(Q^2/\Lambda_{QCD}^2)} \quad (2.2)$$

where  $\Lambda_{QCD}$  is the QCD confinement scale and  $n_f$  is the number of fermion flavors with mass below  $Q$ . Since the mass  $m \gg \Lambda_{QCD}$  and the coupling constant  $\alpha_s \ll 1$ , the process, will be occurred. However, this model works only for the lowest quarkonium states. The charm quark is an elementary fermion with spin  $\frac{1}{2}$ , thus the spin-dependent effects are considered. There are three spin interactions as following equation:

$$V(r) = V_{LS}(r)(\vec{L} \cdot \vec{S}) + V_T(r) \left[ S(S+1) - \frac{3(\vec{S} \cdot \vec{r})(\vec{S} \cdot \vec{r})}{r^2} \right] + V_{SS}(r) \left[ S(S+1) - \frac{3}{2} \right], \quad (2.3)$$

where the spin-orbit,  $V_{LS}$ , and the tensor,  $V_T$ , terms describe the fine structure of the states, and  $V_{SS}$  is the spin-spin interaction (Voloshin, 2008).

## 2.2 Previous charmonium studies

The charm particle is an one of elementary particle in the standard model which provides unique opportunities for probing the strong and weak interaction. The charm quark can only decay via weak decays, mediated by a  $W^\pm$ -boson, into a strange or down quark.

There are many experiments doing research on charm particle. The first charm quark was found in the discovery of the  $J/\psi$  at Brookhaven National Laboratory's 30-GeV alternating-gradient synchrotron (Aubert et al., 1974) on Novem-

ber 1974 which is known as the November Revolution and this discovery confirmed the existence of the fourth quark.  $J/\psi$  is  $c\bar{c}$  bound state. Their observation was made from the reaction  $p + \text{Be} \rightarrow e^+ + e^- + x$  by measuring the  $e^+e^-$  mass spectrum. The next discovery of charm particle was in the usual open charm, i.e. D-mesons ( $D^0$  and  $D^+$ ) which is the lightest particle containing charm quarks. There are three laboratories that have done the research on this particle.

1. **BaBar collaboration** - Observation of a Narrow Meson Decaying to  $D_s^+\pi^0$  at a Mass of  $2.32 \text{ GeV}/c^2$  (Aubert et al., 2003).
2. **CLEO collaboration** - Observation of a Narrow Resonance of Mass  $2.46 \text{ GeV}/c^2$  Decaying to  $D_s^{*+}\pi^0$  and Confirmation of the  $D_{sJ}^*$  (2317) State (Besson et al., 2003).
3. **Belle collaboration** - Measurements of the  $D_{sJ}$  resonance properties produced in continuum  $e^+e^-$  annihilation near  $10.6 \text{ GeV}$  center-of-mass energy (Mikami et al., 2004).

From above publication, all of them used  $e^+e^-$  annihilation data at energies near  $10.6 \text{ GeV}$  but limited precision results are available, because of the low production cross-section (Teklishyn, 2014).

Nowadays, the LHC can reach collision energies up to  $13 \text{ TeV}$  which provides particles containing bottom quark and these particles produce charmonium via electroweak decay. Thus, using data from ALICE experiment can provide the inclusive production of charmonium from initial hard scattering process and bottom-hadron decay.

## 2.3 Charmonium production

There are two main charmonium production mechanisms. Prompt production occurs in the primary parton interaction when their invariant mass  $m$  much larger than the QCD confinement scale  $\Lambda_{QCD}$ . Secondary charmonium comes from the electroweak decays of b-hadrons, see figure 2.1.

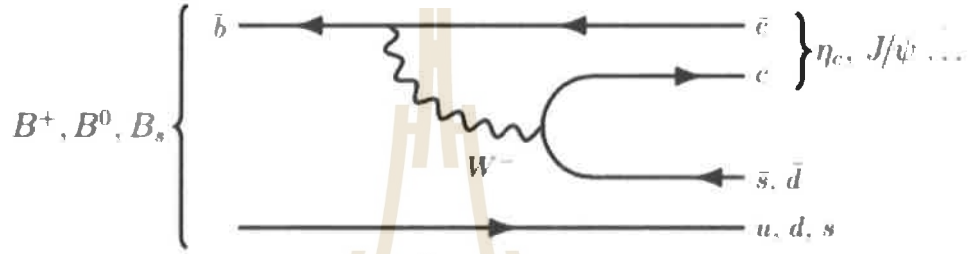


**Figure 2.1** The diagram of the charmonium production from a B-meson decay (Teklishyn, 2014).

## 2.4 Decay modes

The particles containing charm quark that we aimed to study is charmed eta meson ( $\eta_c$ ). A  $\eta_c$  is the lightest charmonium state that can decay to stable hadron as final state as shown in table 2.1. Our interesting decay channel is  $p\bar{p}$ , because this channel is two-body decay which all charmonium can decay to this mode. Table 2.2 shows the list of charmonium states decaying into a proton-antiproton pair as final.  $\eta_c$  has the second largest branching ratio into this decay channel. It is a relatively clean decay channel and the huge amount of data on tape from the ALICE collaboration, where no one have ever done an analysis before. So, this will be an appropriate but challenging research project.



**Table 2.1** List of charmed eta meson decay modes (Tanabashi et al., 2018).

$\eta_c(1S)$ decay mode	branching ratio( $\Gamma_i/\Gamma_{total}$ )
$K\bar{K}\eta$	$(7.3 \pm 0.5)\%$
$\eta\pi^+\pi^-$	$(1.7 \pm 0.5)\%$
$K^+K^-\pi^+\pi^-\pi^0$	$(3.5 \pm 0.6)\%$
$3(\pi^+\pi^-)$	$(1.8 \pm 0.4)\%$
$p\bar{p}$	$(1.52 \pm 0.16) \times 10^{-3}$
$p\bar{p}\pi^0$	$(3.6 \pm 1.3) \times 10^{-3}$
$\Lambda\bar{\Lambda}$	$(1.09 \pm 0.24) \times 10^{-3}$

**Table 2.2** List of charmonium states decaying into a proton-antiproton pair as final state (Tanabashi et al., 2018).

	mass, MeV/c <sup>2</sup>	$I^G J^{PC}$	$\mathcal{B}_{c\bar{c} \rightarrow p\bar{p}} \times 10^{-3}$
$\eta_c(1S)$	$2983.9 \pm 0.5$	$0^+(0^{+-})$	$1.52 \pm 0.16$
$J/\psi(1S)$	$3096.900 \pm 0.006$	$0^-(1^{--})$	$2.121 \pm 0.029$
$\chi_{c0}(1P)$	$3414.71 \pm 0.30$	$0^+(0^{++})$	$0.221 \pm 0.008$
$\chi_{c1}(1P)$	$3510.67 \pm 0.05$	$0^+(1^{++})$	$0.076 \pm 0.003$
$h_c(1P)$	$3525.38 \pm 0.11$	$0^-(1^{-+})$	$< 0.15$
$\chi_{c2}(1P)$	$3556.17 \pm 0.07$	$0^+(2^{++})$	$0.073 \pm 0.003$

# CHAPTER III

## THE ALICE EXPERIMENT

A Large Ion Collider Experiment (ALICE) is one of main projects of Large Hadron Collider (LHC) located at the border between France and Switzerland. The objective of this experiment is study the physics of Quark-Gluon Plasma (QGP) which is a state of matter where quarks and gluons are freed. To observe this phenomenon, they have different layers of detectors to measure the particles flying out from heavy ions collision and other collisions, such as Inner Tracking System (ITS), Time Projection Chamber (TPC), Time of Flight (TOF) detector.

### 3.1 Large Hadron Collider (LHC)

Large Hadron Collider (LHC) is one of the largest high energy physics devices that consist of particle accelerator and particle detector. To produce the particle physics study and to understand mystery of the interaction of matter in our universe. The LHC is build at the European Organization for Nuclear Research (CERN), near Geneva, Switzerland. The LHC has been designed to collide proton beam, with maximum center-of-mass energy of 14 TeV at a luminosity of  $10^{34} \text{ cm}^{-2}\text{s}^{-1}$ , as well as Lead (Pb) ions with a maximum energy of 2.8 TeV per nucleon at a peak luminosity of  $10^{27} \text{ cm}^{-2}\text{s}^{-1}$ .

### 3.2 ALICE detector

A Large Ion Collision Experiment (ALICE) is one of main experiment at the LHC. The main propose of ALICE is study the physics of strong interaction of

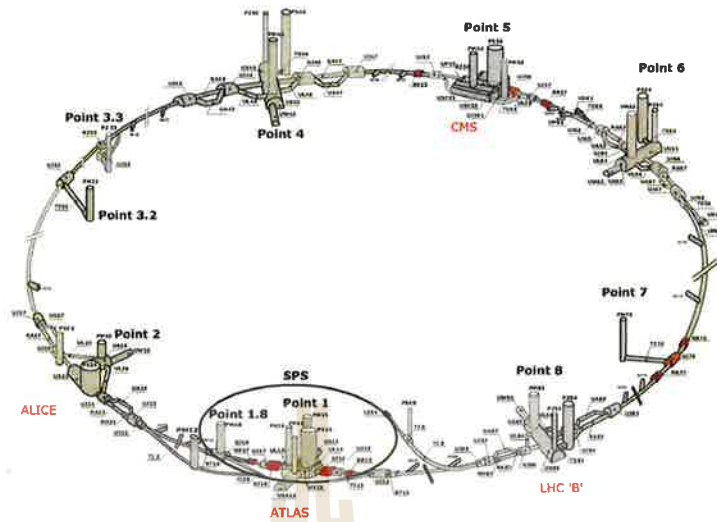


**Figure 3.1** The schematic of the layout of the LHC including each of main experiments (Michel, 2020).

matter and the Quark Gluon Plasma (QGP) by means of a comprehensive study of hadrons, electrons, muons, and photons produced in the collision of heavy nuclei (Pb–Pb), by collision of ions and heavy ions in the middle of detector.



**Figure 3.2** The schematic of ALICE detector (Tauro, 2017).

### 3.2.1 Inner Tracking System(ITS)

The Inner Tracking System (ITS) is a tracking detector closest to beam which is built for tracking particles and reconstructing vertex of particle decay with a very high spatial accuracy. It is also able to contribute to particle identification of low-momentum particles, and improve the momentum resolution of the Time Projection Chamber (TPC).

This detector consists of a six-layer silicon detector divided in three types of detector, with each sub-detector composed of two layers, where the inner two layers closest to beam pipe are the Silicon Pixel Detector (SPD), the middle two layers are the Silicon Drift Detector (SDD), and the outer two layers is the Silicon Strip Detector (SSD). The schematic of these three types of silicon detectors as shown in figure 3.5. The detection of particle covers the rapidity range of  $|\eta| < 0.9$  for all vertices located within the length of the interaction diamond ( $\pm 1\sigma$ , i.e.  $\pm 5.3$  cm along the beam direction). The number, position and segmentation of the layers were optimized for efficient track finding and high impact-parameter resolution.

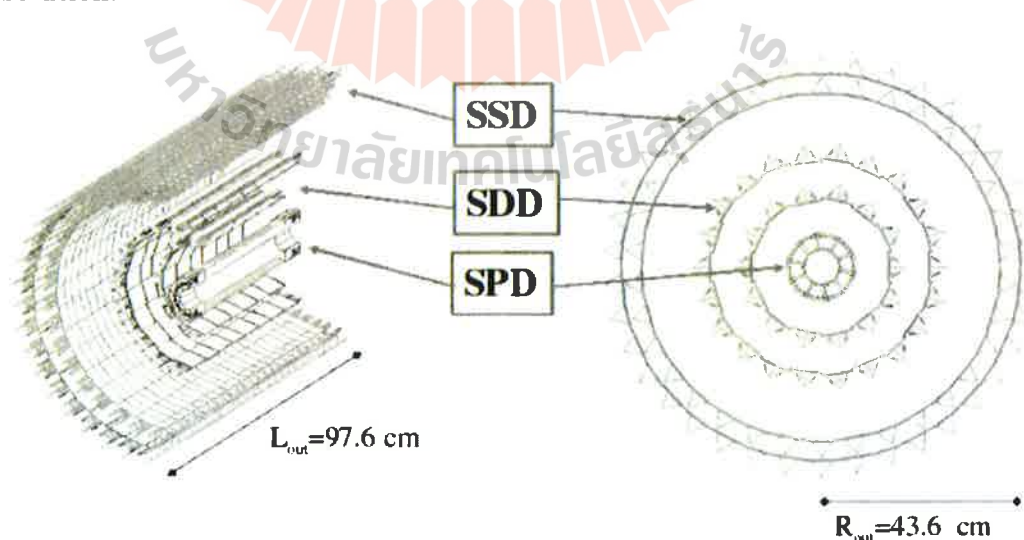


**Figure 3.3** The schematic of ITS layers (The ALICE Collaboration et al., 2008).

In 2019-2020, the ALICE collaboration will upgrade the ITS during LHC Long Shutdown 2 to use it in the experiment after that in Run 3. The Suranaree University of Technology helped ALICE to improve a silicon sensor to detect non-accessible particles within the previous ITS, for example D and  $J/\psi$  mesons and  $\Lambda_c^+$  baryons. This due to the fact that they contain heavy quarks, like charm and bottom, and thus have a relatively short lifetime. After ITS upgrade, SUT plans to do data analysis on charmed lambda baryon ( $\Lambda_c^+$ ). So before upcoming new results, this research will be a starting point of data analysis project in the future.

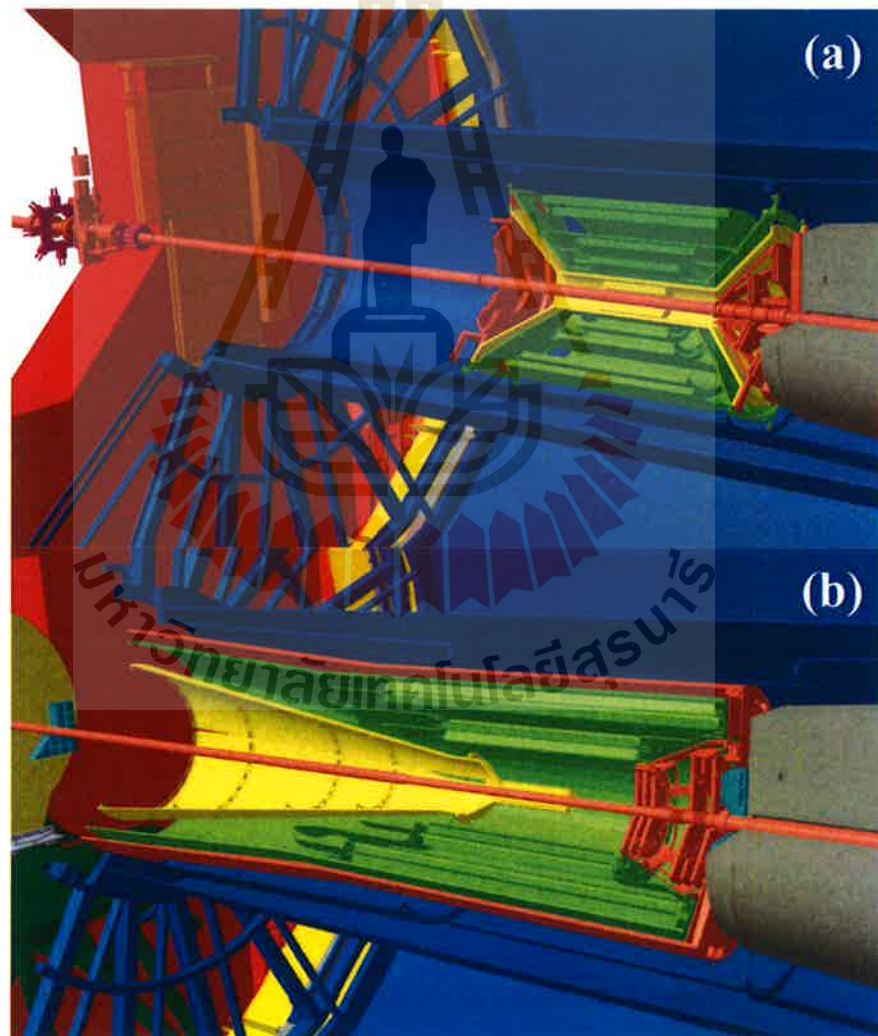


**Figure 3.4** Schematics of the Inner Tracking System during (a) Run 2 and (b) Run 3 (Tauro, 2017).

### 3.2.2 Time Projection Chamber (TPC)

The Time Projection Chamber (TPC) is the main tracking detector in the central barrel of ALICE and is optimised together with the other central barrel detectors to provide charged-particle momentum measurements with good two-track separation, particle identification, and vertex determination with a wide momentum range. It covers the full azimuthal range and a pseudorapidity coverage of  $|\eta| < 0.9$  for the full radial track length, with the active volume spanning a radial position of  $848 < r < 2466$  mm, and a large  $p_T$  is covered from low  $p_T$  of about 0.1 GeV/c up to 100 GeV/c with good momentum resolution.

This detector consists of a large cylindrical field cage filled with 90 m<sup>3</sup> of a gas mixture of primarily Ar or Ne. When charged particles propagate through the TPC, they ionise the medium gas and provide electrons, that drifts at a speed of 2.7 cm/ $\mu$ s under the large voltage towards the multi-wire proportional chambers (MWPCs), as a readout cathode on the end plates. The position of the charged deposition on the cathode gives the two dimensional track position in  $r\phi$ , and the time taken for the electrons to drift to the end plates gives the track position in z-axis.

### 3.2.3 Time of Flight Detector (TOF)

The Time-Of-Flight detector is a large array of Multi-gap Resistive Plate Chambers (MRPCs), covering the full azimuthal range with a rapidity coverage of  $|\eta| < 0.9$ . It provides particle identification in the intermediate momentum range, below about 2.5 GeV/c for pions and kaons, up to 4 GeV/c for protons, via the measurement of the time of flight of charged particles from the interaction point to the TOF. The TOF work together with the ITS and TPC for track and vertex reconstruction and for  $dE/dx$  measurements in the low-momentum range,

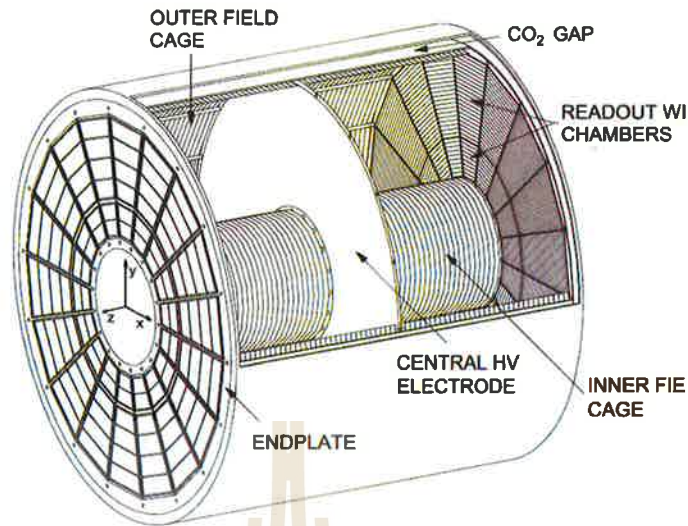


**Figure 3.5** Schematic drawing of the ALICE TPC (Alme et al., 2010).

which provides event-by-event identification of large samples of pions, kaons, and protons.

### 3.3 Detector performance

#### 3.3.1 Tracking

The procedure of particle track finding of central barrel tracking in ALICE detector is shown in figure 3.6. First step is clusterization, which the data collecting from detector are converted into “clusters” characterized by positions, signal amplitudes, signal times, etc., and their associated errors. The clusterization is performed separately for each detector. The next step is to determine the preliminary interaction vertex using clusters in the first two ITS layers (SPD). Subsequently, track finding and fitting is performed in TPC and ITS using the Kalman filter technique. The found tracks are matched to the other central barrel detectors and fitted.

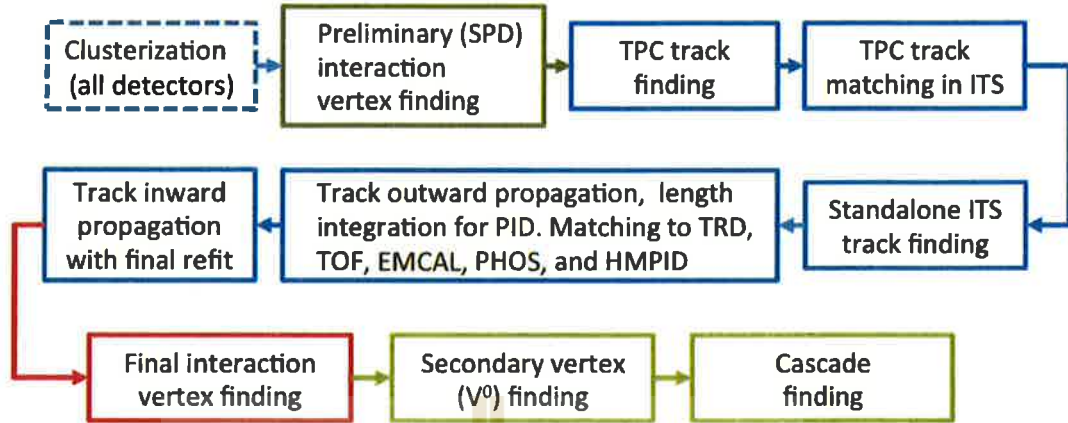


**Figure 3.6** Event reconstruction flow in central barrel tracking (Alice Collaboration, 2014).

### 3.3.2 Particle Identification (PID)

The particle identification in ALICE can either be performed using a single detector, or using a combination of the signals from more than one detector to optimize identification. In a traditional way, the PID can be done using number-of-sigma ( $n\sigma$ ) approach, where a selection is made on the difference between the measured signal from the detector  $S$  and the expected response from the detector  $\hat{S}$  given a particle species hypothesis  $H_i$ , divided by the detector resolution  $\sigma_i$  where  $n\sigma = (S - \hat{S}(H_i))/\sigma_i$ . This can be done for multiple detectors to cover different kinematic regions and particle type.

The TPC performs the PID via measurement of the energy loss per unit length  $dE/dx$ , or specific energy loss, which is related to the number of measured electrons ionised by the charged particle propagating through the TPC. The specific energy loss of a given particle is described by the Bethe-Bloch formula, and in ALICE a parameterisation of this formula, which was proposed by the ALEPH



collaboration (Blum et al., 2008). The formula can be written as

$$f(\beta\gamma) = \frac{P_1}{\beta^{P_4}} \left( P_2 - \beta^{P_4} - \ln \left( P_3 + \frac{1}{(\beta\gamma)^{P_5}} \right) \right), \quad (3.1)$$

where  $P_{1-5}$  are parameters from fitting measured specific energy loss. The figure 3.7 shows the specific energy loss of measured tracks in proton-proton collision as function of the track momentum, along with the Bethe-Bloch characterisations for different charged particles, which can clearly be seen a separation between the particle species.

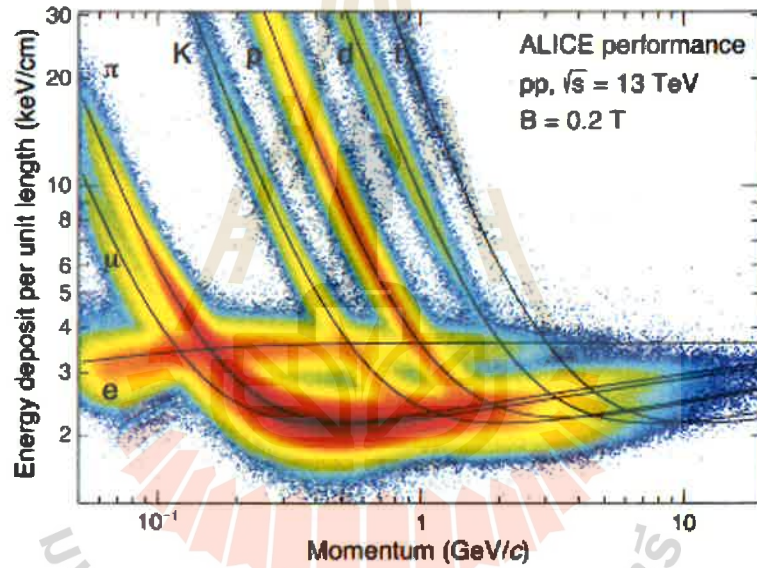


**Figure 3.7** Specific energy loss ( $dE/dx$ ) versus particle momentum in the TPC in pp collisions at  $\sqrt{s} = 13$  TeV. The lines show the parametrizations of the expected mean energy loss (ALICE collaboration, 2015).

The PID capabilities of the TOF detector is shown in figure 3.8, where the velocity of particle as a fraction of the speed of light  $\beta$  is plotted as a function of momentum.

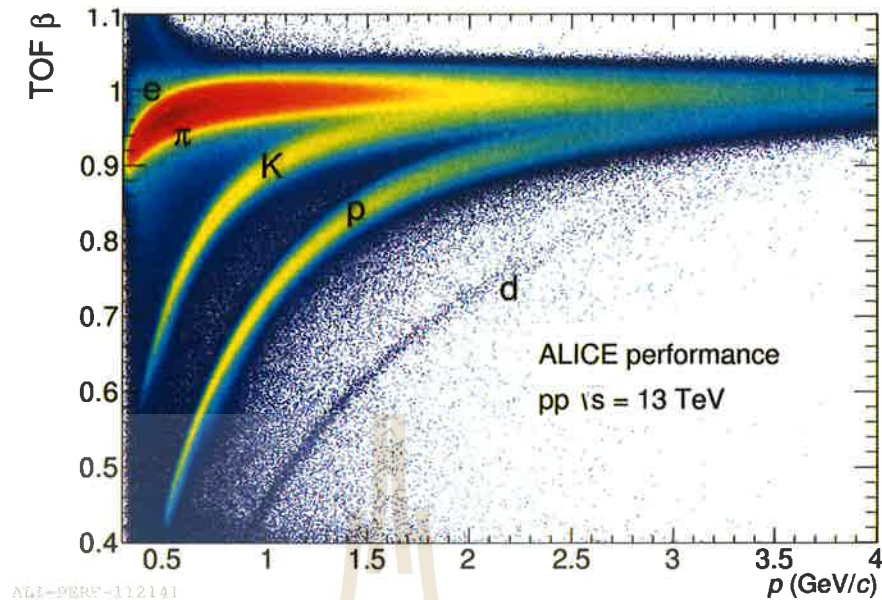


**Figure 3.8** TOF beta vs momentum performance plot in pp collisions at 13 TeV (ALICE collaboration, 2020).

### 3.4 ALICE analysis

#### 3.4.1 AliRoot/AliPhysics, the ALICE analysis framework

AliRoot uses the ROOT (CERN Collaboration, 2014) software as a foundation on which the framework for simulation, reconstruction and analysis is built for high-energy physics experiments. The GEANT3, GEANT4, and FLUKA packages perform the transport of particles through the detector and simulate the energy deposition from which the detector response can be simulated. Except for large existing libraries, such as Pythia6 and HIJING, and some remaining legacy code, this framework is based on the Object Oriented programming paradigm, and is written in C++.

AliPhysics is software repository of the Physics Board which coordinates data analysis via the Physics Working Groups (PWGs) (ALICE Collaboration, 2019). At present, the following PWG have started their activity:

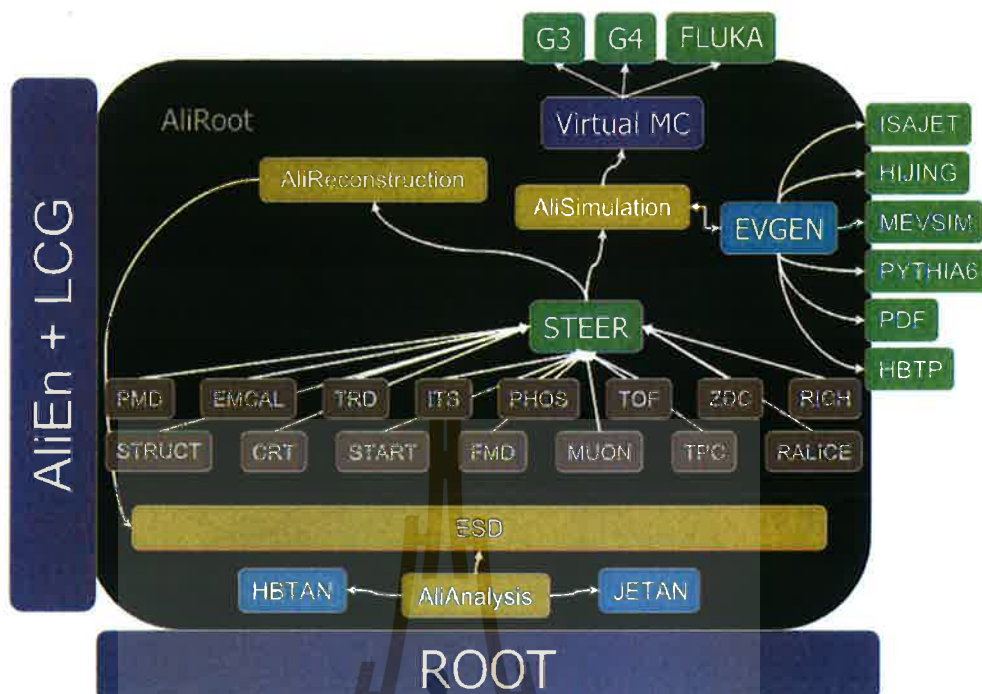


**Figure 3.9** The general schema of the AliRoot architecture (CERN Accelerating science, 2011).

- PWG-CF - Correlations and Flow;
- PWG-DQ - Dileptons and Quarkonia;
- PWG-GA - Neutral Mesons decaying into photons;
- PWG-HF - Heavy Flavour;
- PWG-JE - Jets;
- PWG-LF - Light Flavour Spectra;
- PWG-PP - Physics Performance;
- PWG-UD - Ultraperipheral collisions and Diffraction;
- PWG-MM - Monte Carlo generators and Minimum Bias physics;

In this research, we will use software from two groups, the PWG-DQ for the charmonium analysis, and the PWG-LF for the proton-antiproton invariant mass spectra.



# CHAPTER IV

## ANALYSIS OF CHARMONIUM DECAY TO PROTON-ANTIPROTON PAIR

### 4.1 Analysis Overview

The measurement of charmonium was performed by searching the pairs of  $p$  and  $\bar{p}$  from  $pp$  collisions at  $\sqrt{s} = 13$  TeV with the ALICE experiment. The result of particle collisions from the ALICE detector are stored in the ALICE GRID. The first section details the process of retrieving the experiments data from the ALICE GRID using AliRoot framework. After the data has been collected, the next step is the selection of  $p$  and  $\bar{p}$  candidates for reconstructing the four momentum vector of the charmoniums and invariant mass by energy-momentum conservation. The production yield of charmonium is drowned by the combinatorial background, in section 4.6 show the techniques and result of background subtraction. The last section is signal extraction by using Gaussian function and quadratic function to obtain the signal distribution and residue background, respectively.

### 4.2 Retrieving data from ALICE GRID

All data from experiment are stored in the ALICE GRID as ESDs and AODs files. ESDs are Event Summary Data and AODs are Analysis Object Data (ALICE Collaboration, 2010), both are a tree structure which contains the reconstructed data for each event, namely tracks with particle identification information, i.e. measured momentum together with information such as the measured vertex

position and other so called global event properties.

However, AODs and ESDs require huge storage space about petabytes which is impossible to download these files. The list of run numbers that are provided by  $pp$  collisions in Run 2 from 2016 to 2018, are shown in appendix V. Each of them require time to submit the analysis task for running the calculation. Thus, to reduce the process of calculation on huge data files, a new data structure is introduced for selecting only the specific information that for the analysis at hand. This new data structure called “AliAnalysisCODEX”. it was used for searching exotic hadrons, by selecting necessary information of stable particles from ESDs, such as event properties, the momentum vector of particles, the particle identification of the detector, and significance of the signal.

### 4.3 Event selection of $pp$ collision

After the data was retrieved from ALICE GRID using AliRoot, the next process is the selection of proton and anti-proton for reconstructing the charmonium candidates. First, considering the event properties, to classify the good  $pp$  collision events, there are three criteria:

- The position of the primary vertex along the beam direction is less than 10 centimeter for avoiding TPC limiting plane, where the primary vertex is interaction point of  $pp$  collision.
- Particle multiplicity is higher than zero to confirm that a collision has occurred and there are produced particles.
- The number of protons and antiprotons passing track selection is at least one for each, where the candidate tracks are kept to combine with other events for background subtraction, more explanation in section 4.6.2.

## 4.4 Proton and antiproton track selection

The second step is track selection. The proton and antiproton track candidates in the midrapidity region ( $|\eta| < 0.8$ ) are required to have the following criteria:

### 4.4.1 Track quality requirements in ITS and TPC

To select the proton and antiproton tracks that was reconstructed from the cluster of particle interacting with the tracking systems, such as ITS and TPC.

- There are track hits on the SPD layers of ITS.
- At least 70 in the TPC.
- Quality of track reconstruction,  $\chi^2/\text{ndf} < 4$
- There are track refit in both TPC and ITS.
- The track has no kink.
- A distance of closest approach to primary vertex smaller than 200 mm in  $z$  direction and  $1.05 + 3.5/p_T^{1.1}$  mm in  $xy$  plane.
- Transverse momentum  $p_T > 0.30$  GeV/c.
- Pseudorapidity interval  $|\eta| < 0.8$ .

Here is the explanation of the criteria above. Due to the charmonium being a short-lived particle with a very low decay length ( $\sim 6$  fm), the proton and antiproton tracks have to move pass the first two ITS layers, the SPD. Hence, the track should be triggered by at least 2 ITS layers. For the stable proton and antiproton, both of them have to pass through all the central tracking. To know

that, the track must be detected by TPC with at least 70 number of clusters. This number came from the energy resolution of TPC scaling according to the law  $\sigma_{dE/dx} \propto 1/\sqrt{n}$ , where  $n$  is number of clusters in the TPC (Alme et al., 2010). And the quality of track reconstruction is considered by chi-square of track fitting. For make sure that ITS and TPC detected the same particle, the track is need to be refitted in both ITS and TPC. The track required to have no kink to confirm that the particle do not produce any neutral particle by decays. The distance of closest approach (DCA) is very useful to separate primary, secondary, and background tracks. The secondary tracks are produced by either decays or interactions with the detector, they are unlikely project back to primary vertex. But the secondary protons and antiprotons from the short-lived particles need to point to primary vertex. For the DCAs along beam direction (z-axis) are required to be smaller than 200 mm and the maximum DCAs in transverse plane depend on transverse momentum. To reduce the background tracks, the TOF is required for identifying protons and antiprotons. Hence, the transverse momentum of particle is bigger than 300 MeV/c for reaching the TOF.

#### 4.4.2 Particle identification selection

The charged particle tracks can be classified by using TPC and TOF signals. The TPC measures the total energy loss per unit path length of a charged particle by collecting drifted electrons from the ionized medium. The total energy loss per unit path length is calculated using the Bethe-Bloch formula, which depends on charge and rest mass in a fixed momentum bin. Figure 4.1 shows the energy loss of charged particles vs. their momentum in the TPC.

The TOF is a detector for measuring the time of particles using to pass the detector to detect their velocity ( $\beta$ ) as shown in figure 4.2. The TOF also



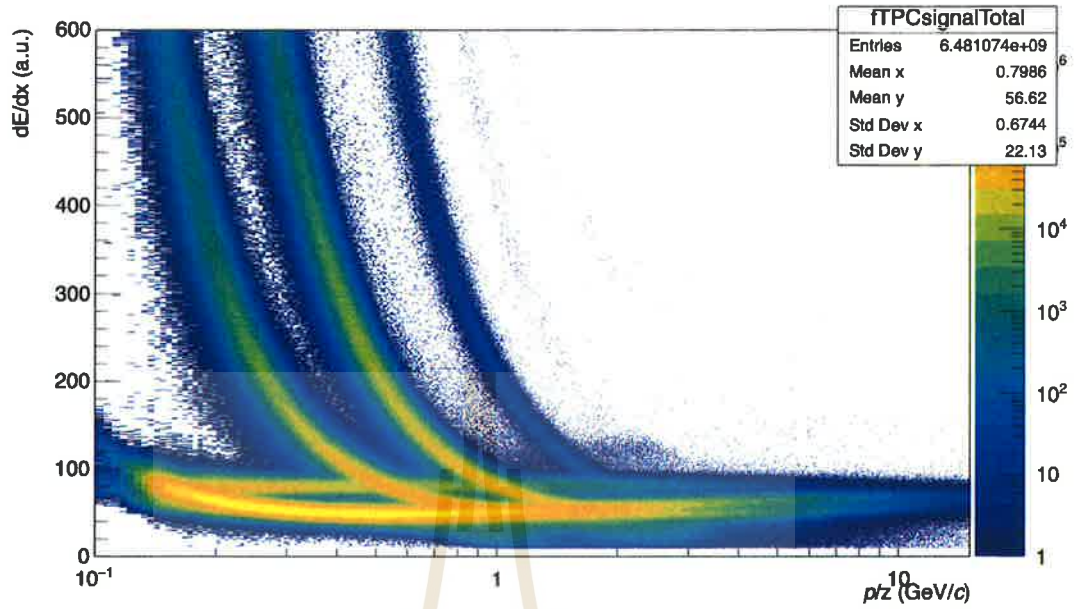


**Figure 4.1** Total  $dE/dx$  spectrum versus TPC momentum in ALICE TPC from  $pp$  collisions at  $\sqrt{s} = 13$  TeV

identify the particle by mass measurement which is determined by its momentum and velocity:

$$m = \frac{p}{\beta\gamma c} \quad (4.1)$$

where  $\beta = v/c$  and  $\gamma = (1 - \beta^2)^{-1/2}$ . But there are various instrumental effects. It is then preferable to calculate the square of the mass of the particle according to

$$m^2 = p^2 \left( \frac{1}{\beta^2} - 1 \right). \quad (4.2)$$

Figures 4.3 and 4.4 show the square of the TOF mass of protons and antiprotons vs. the TPC momentum. The squared mass of these particles is clustered around the square of the exact proton mass, and there are noticeable signals in the TPC momenta around 0.5 - 0.9 GeV/c while squared mass higher than 1 GeV<sup>2</sup>/c<sup>4</sup>.

Before we determine the squared mass of proton and antiproton cut, we

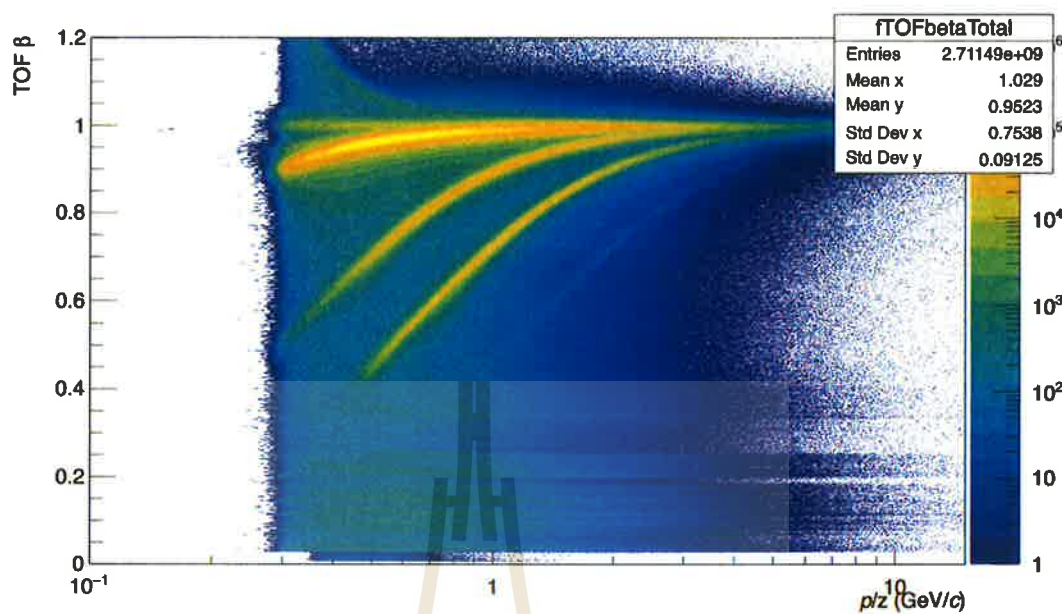


**Figure 4.2** Total TOF speed ( $\beta$ ) versus TPC momentum in ALICE TOF from  $pp$  collisions at  $\sqrt{s} = 13$  TeV.

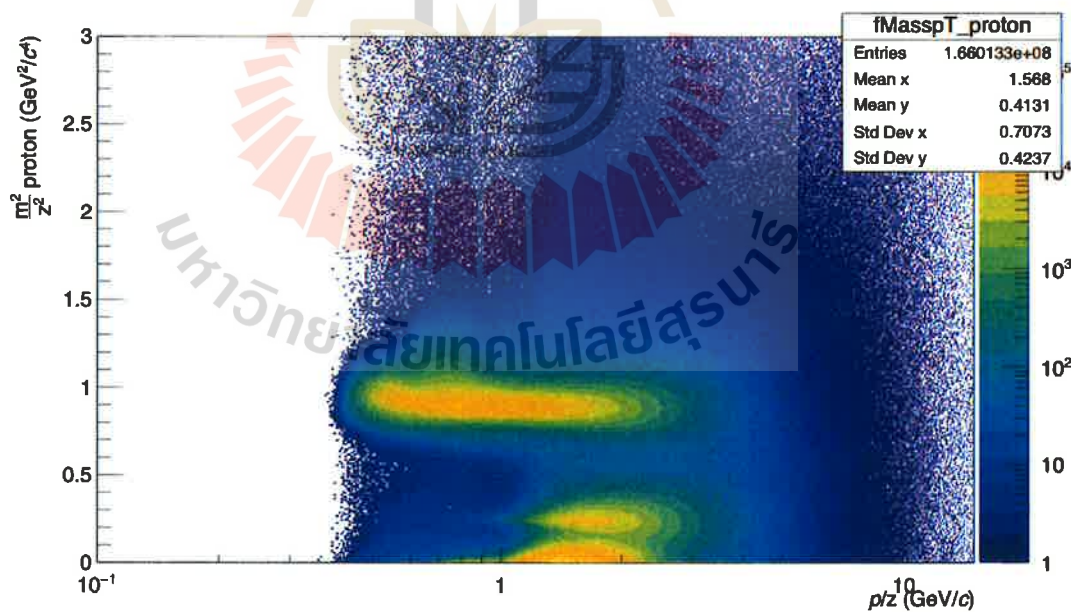


**Figure 4.3** TOF mass of protons in ALICE TOF versus TPC momentum of protons in ALICE TPC.

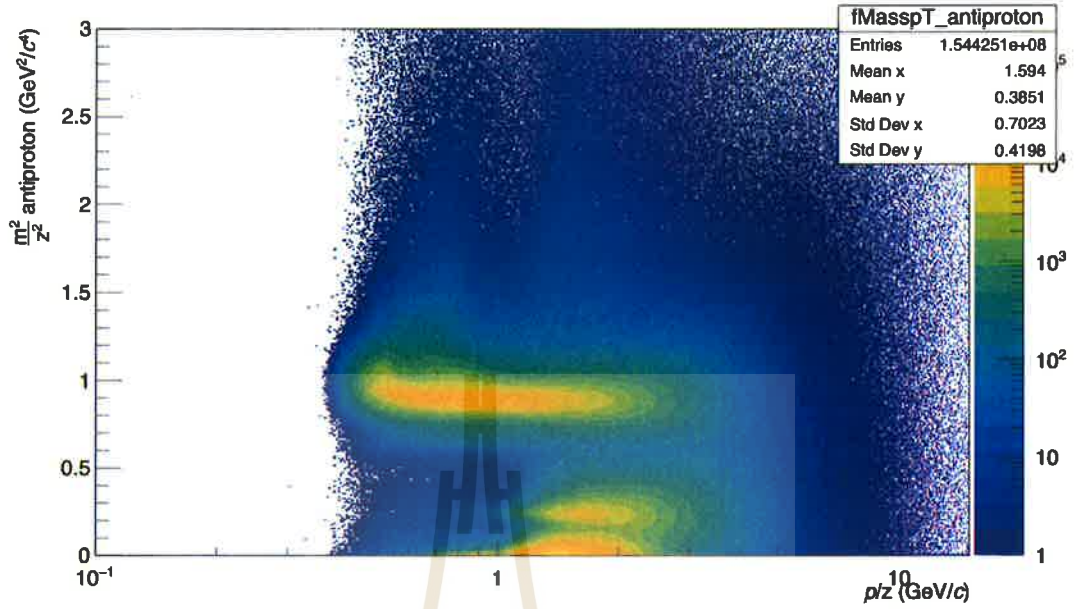


**Figure 4.4** TOF mass of antiprotons in ALICE TOF versus TPC momentum of antiprotons in ALICE TPC.

show in figure 4.5 and 4.6 the number of sigma of signal distribution without squared mass cut in TPC and TOF, respectively. Hereby sigma represent, the standard deviation for a normal distribution used for describing the signal is used to select the confidence interval of the signal and reject the outlier signal. There are noticeable signals from other particles overlapping the proton/antiproton signal at TPC momenta higher than 1 GeV/c for both  $n\sigma_{TPC}$  and  $n\sigma_{TOF}$ . To reduce these non-proton signals, we decide to use the loose squared mass interval cut between 0.7 - 1.1 GeV<sup>2</sup>/c<sup>4</sup>.

The results of both TPC and TOF signals after using squared mass cut, is shown in figures 4.9 and 4.10. The result of  $n\sigma_{TPC}$  and  $n\sigma_{TOF}$  is shown in figures 4.7 and 4.8. We see that the signals in TPC still have the noticeable non-proton background while the signals in TOF are much cleaner.

Figure 4.11 shows the relation between  $n\sigma_{TPC}$  and  $n\sigma_{TOF}$ . Normally, the

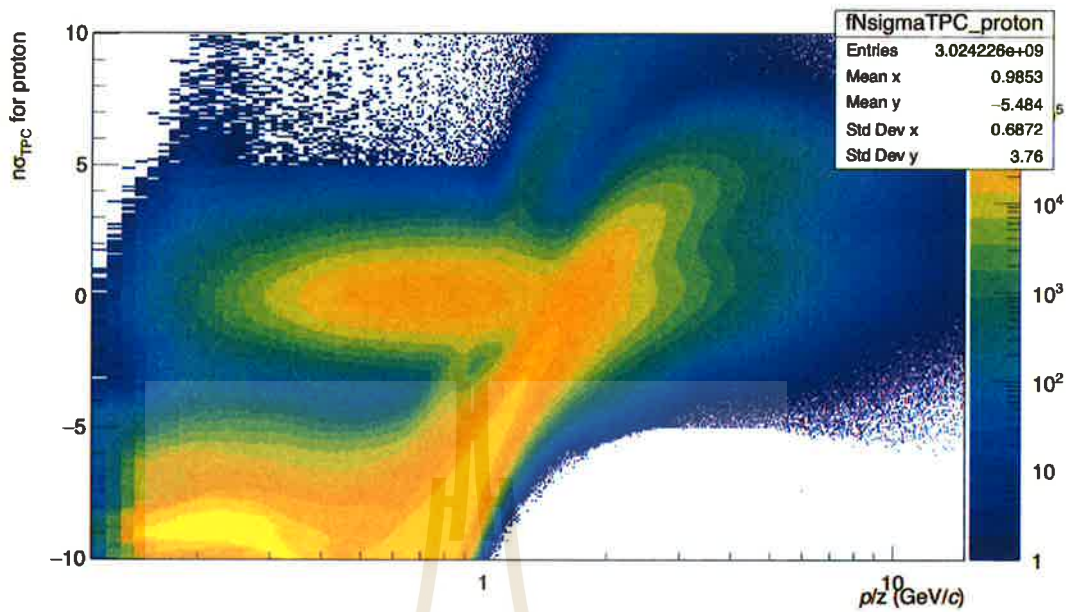


Figure 4.5  $n\sigma_{TPC}$  of proton's signals in ALICE TPC versus TPC momentum.

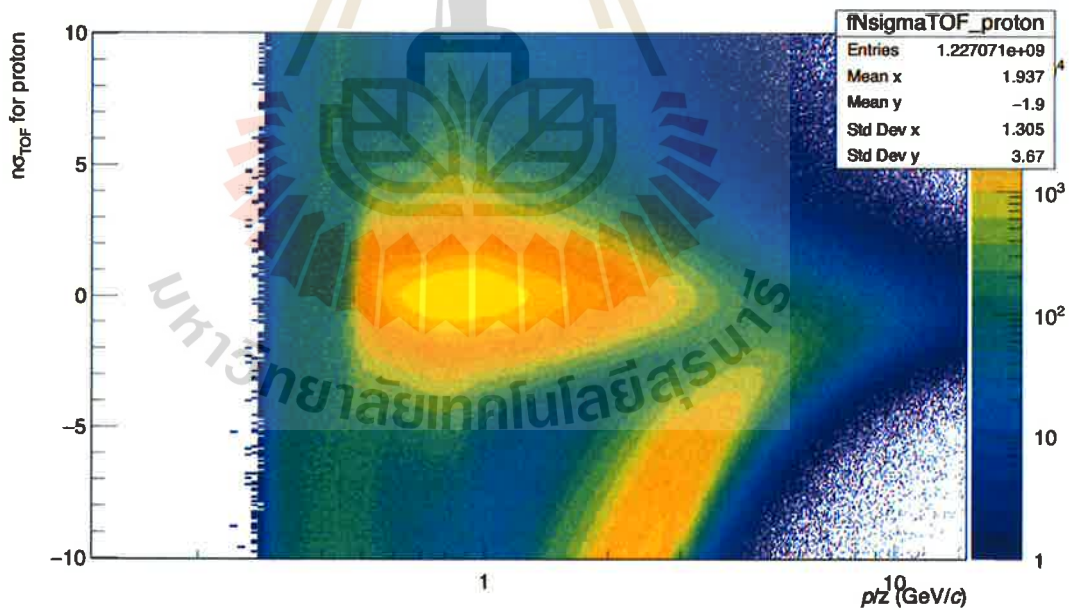


Figure 4.6  $n\sigma_{TOF}$  of proton's signals in ALICE TOF versus TPC momentum.

general cut for number of sigmas is 3, but we want to reduce the background from non-protons in TPC. So we use 2 sigmas for the TPC signal. For the TOF signal,

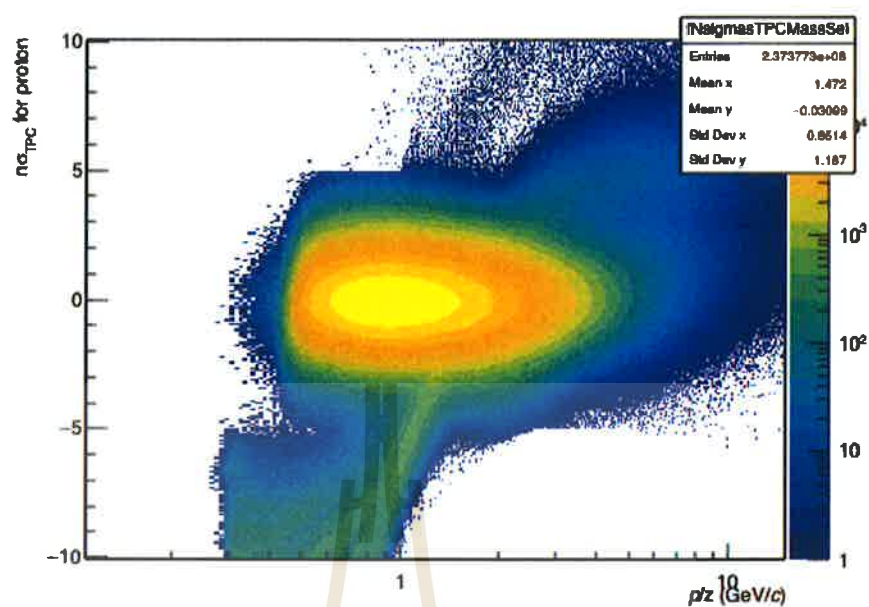


Figure 4.7  $n\sigma_{TPC}$  of proton and antiproton signal in ALICE TPC with the squared mass in the range between 0.7 - 1.1  $\text{GeV}^2/c^4$  versus TPC momentum.

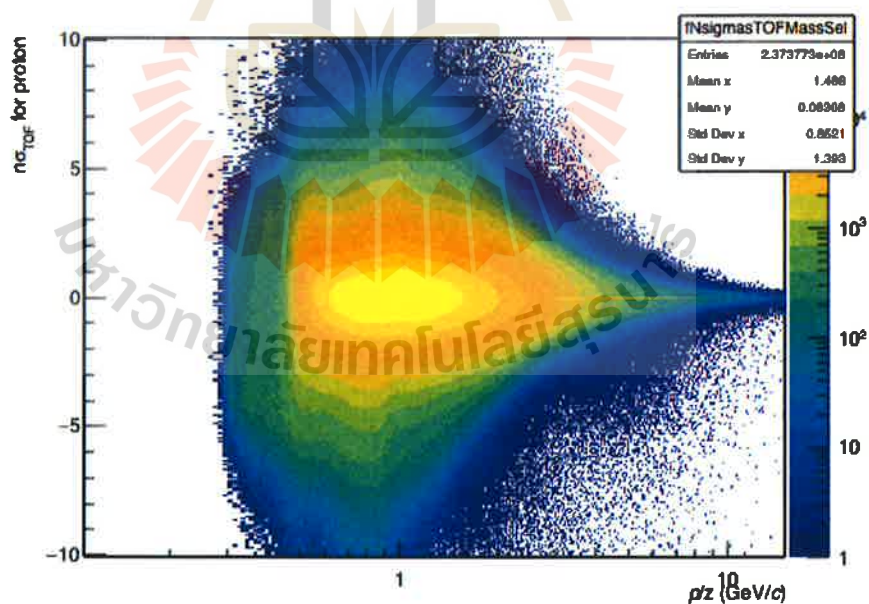
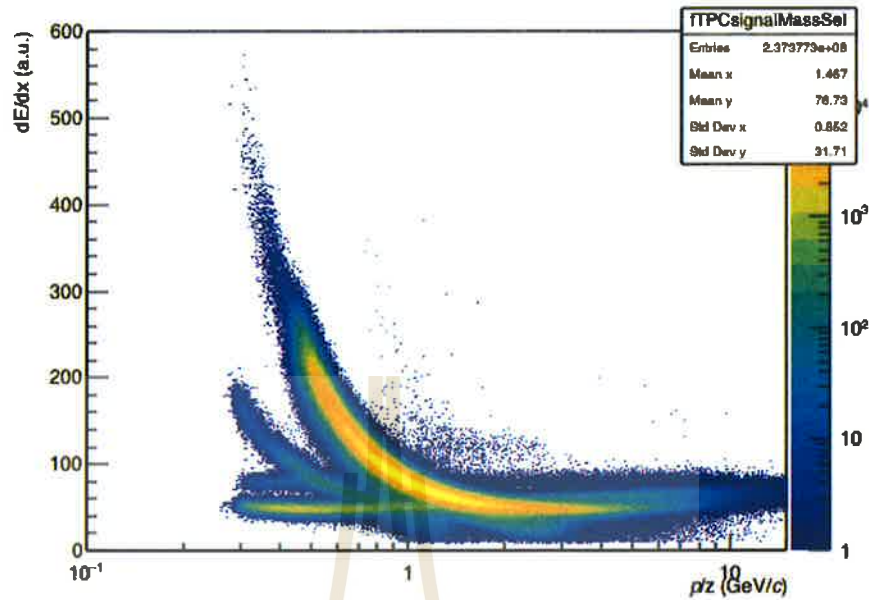


Figure 4.8  $n\sigma_{TOF}$  of proton and antiproton signal in ALICE TOF with the squared mass in the range between 0.7 - 1.1  $\text{GeV}^2/c^4$  versus TPC momentum.



**Figure 4.9** Total  $dE/dx$  spectrum with the squared mass in the range between  $0.7 - 1.1 \text{ GeV}^2/c^4$  versus TPC momentum in ALICE TPC from  $pp$  collisions at  $\sqrt{s} = 13 \text{ TeV}$

we want to collect all possible proton, we therefore use 5 sigmas for the TOF signal.

#### 4.5 Charmonium candidates selection using invariant mass reconstruction

To study short lived particles, the invariant mass is the main variable to identify the interesting particles from a ton of particle moving out in each collision event. Invariant mass is the mass of the particle in any frame which can be calculated by measuring particle's energy  $E$  and its momentum  $\vec{p}$ . Consider the two-body decay process illustrated in figure 4.14. The parent particle has an unknown four-momentum  $p_p$ , and the decay products have 4-momenta  $p_1$  and  $p_2$ . From Energy-momentum conservation, the sum of the 4-momenta of the decay

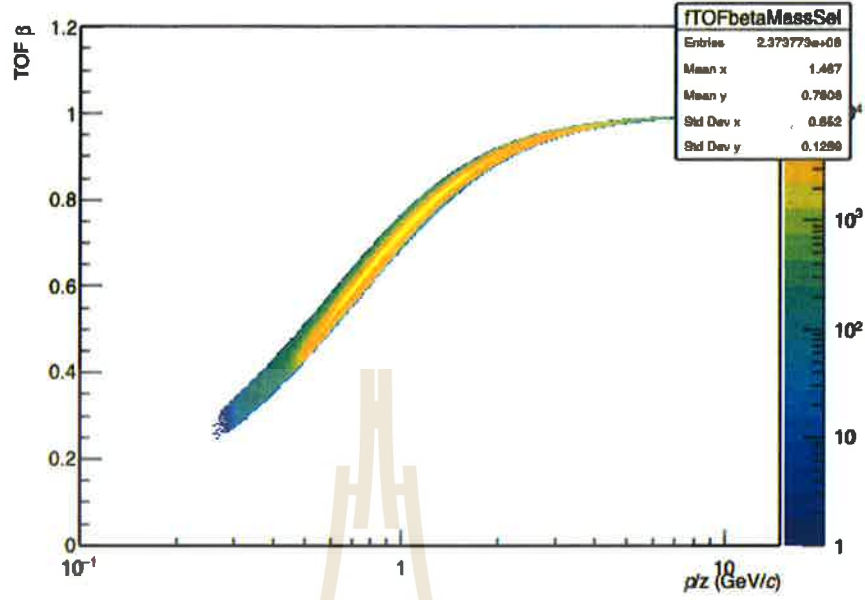


**Figure 4.10** Total TOF speed ( $\beta$ ) versus with the squared mass in the range between 0.7 - 1.1  $\text{GeV}^2/c^4$  versus TPC momentum in ALICE TOF from  $pp$  collisions at  $\sqrt{s} = 13$  TeV.

products equals the four-momentum of the parent particle:

$$p_p = p_1 + p_2 = (E_1 + E_2, \vec{p}_1 + \vec{p}_2). \quad (4.3)$$

The square of the 4-momentum  $p_p$  provides the square of the mass,  $m_p$ , of the parent particle. A measurement of the momenta of the decay products and calculation of the square of the sum of their 4-momenta can identify the parent particle species. The mass of the parent particle is given by the square of  $p_p$ :

$$\begin{aligned} p_p^2 &= m_p^2 = (E_1 + E_2)^2 - |\vec{p}_1 + \vec{p}_2|^2, \\ m_p^2 &= E_1^2 + 2E_1E_2 + E_2^2 - |\vec{p}_1|^2 - |\vec{p}_2|^2 - 2\vec{p}_1 \cdot \vec{p}_2, \\ &= m_1^2 + m_2^2 + 2E_1E_2 - 2\vec{p}_1 \cdot \vec{p}_2. \end{aligned} \quad (4.4)$$

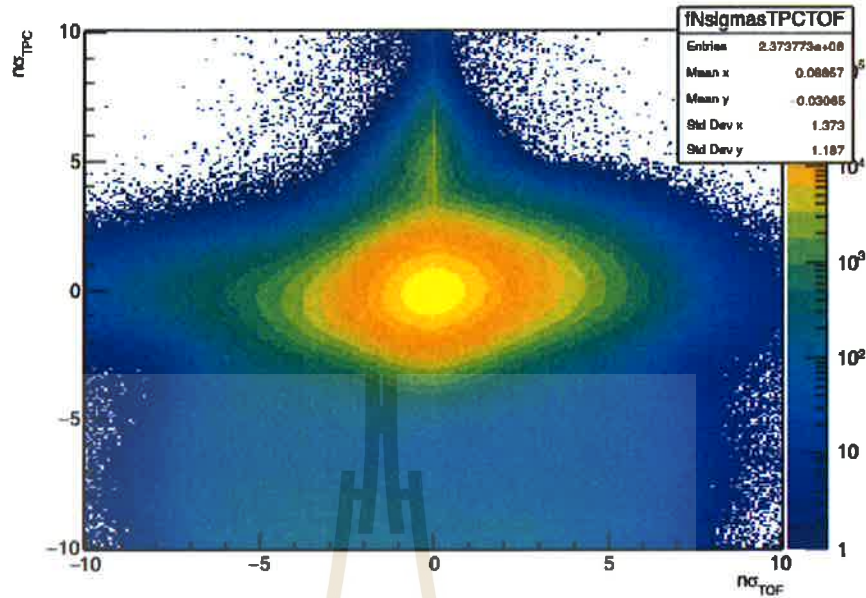


**Figure 4.11** The relation between  $n\sigma_{TPC}$  and  $n\sigma_{TOF}$  of proton/antiproton track that is measured by ALICE TPC and TOF from  $pp$  collisions at  $\sqrt{s} = 13$  TeV.

## 4.6 Combinatorial Background Estimation

The charmonium candidates are reconstructed from all possible pairs of protons and antiprotons, including correlated pairs that came from charmonium decay, and uncorrelated pairs, for example, there are  $N$  charmoniums produced in an event, that decay into  $N^+$  protons and  $N^-$  antiprotons, there are  $N^+N^- = N^2$  charmonium candidates and  $N^2 - N$  combinatorial background. In real experimental events there is a huge background of protons and antiprotons not only stemming from the decay of charmed eta mesons, but e.g. from weak decays of hyperons or from spallation processes with the detector material. Since the amount of background sources is large compared to the number of signal events. It is challenging to find the of signals within the sea of background. The importance of the background reduction is to increase the significance of signals, which is calculated by:



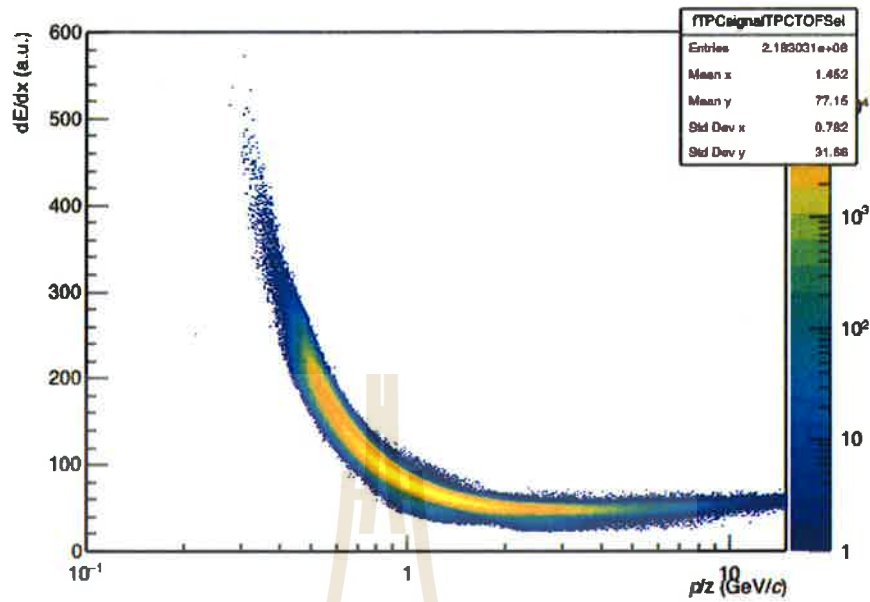


**Figure 4.12** Total  $dE/dx$  spectrum with the squared mass in the range between  $0.7 - 1.1 \text{ GeV}^2/c^4$ ,  $|n\sigma_{TPC}| < 2$ , and  $|n\sigma_{TOF}| < 5$  versus TPC momentum in ALICE TPC from  $pp$  collisions at  $\sqrt{s} = 13 \text{ TeV}$

$$\text{Significance} = \frac{S}{\sqrt{S+B}}, \quad (4.5)$$

where  $S$  is number of investigated signals given by integrating of signal distribution over the confident interval, and  $B$  is number of the background under the signal distribution in the same range. In the ideal, if the estimated background provide a similar shape to the spectrum and get rid of the rest background, the best significance is equal to  $S/\sqrt{S}$ . Otherwise, if the background are a lot more than the number of signal, the significance become zero.

To optimize the signal for high significance, there are three techniques to reproduce the uncorrelated pairs distribution to subtract background.

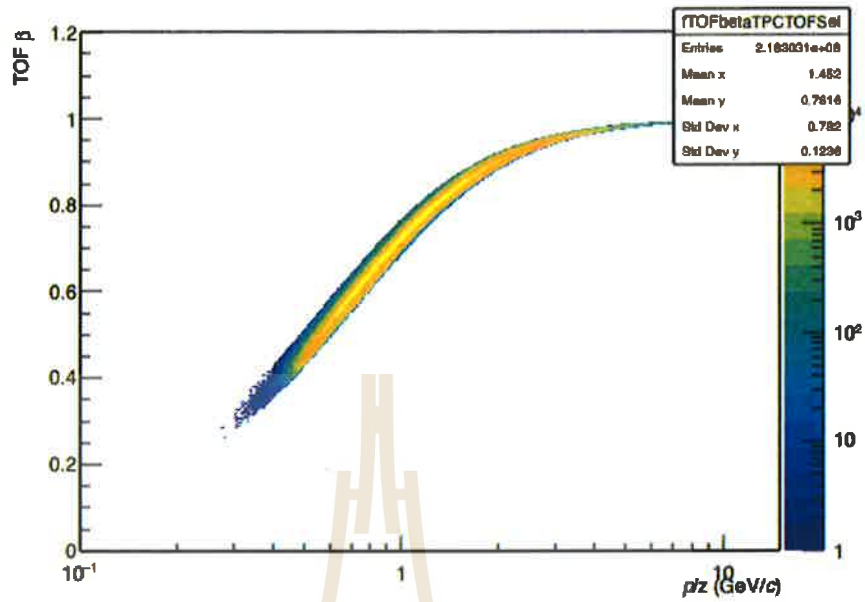


**Figure 4.13** Total TOF speed ( $\beta$ ) versus with the squared mass in the range between  $0.7 - 1.1 \text{ GeV}^2/c^4$ ,  $|n\sigma_{TPC}| < 2$ , and  $|n\sigma_{TOF}| < 5$  versus TPC momentum in ALICE TOF from  $pp$  collisions at  $\sqrt{s} = 13 \text{ TeV}$ .

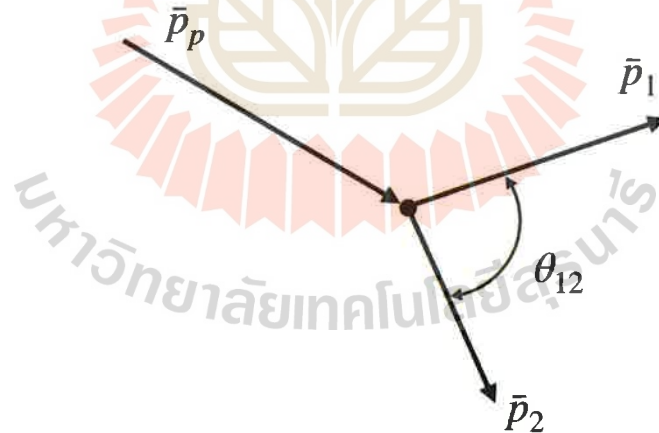


**Figure 4.14** Kinematics of two-body decays and invariant mass reconstruction.

#### 4.6.1 Like-sign pair method

The invariant mass spectrum of charmonium is reconstructed from protons and antiprotons, where both have the same properties except their charge, the so-

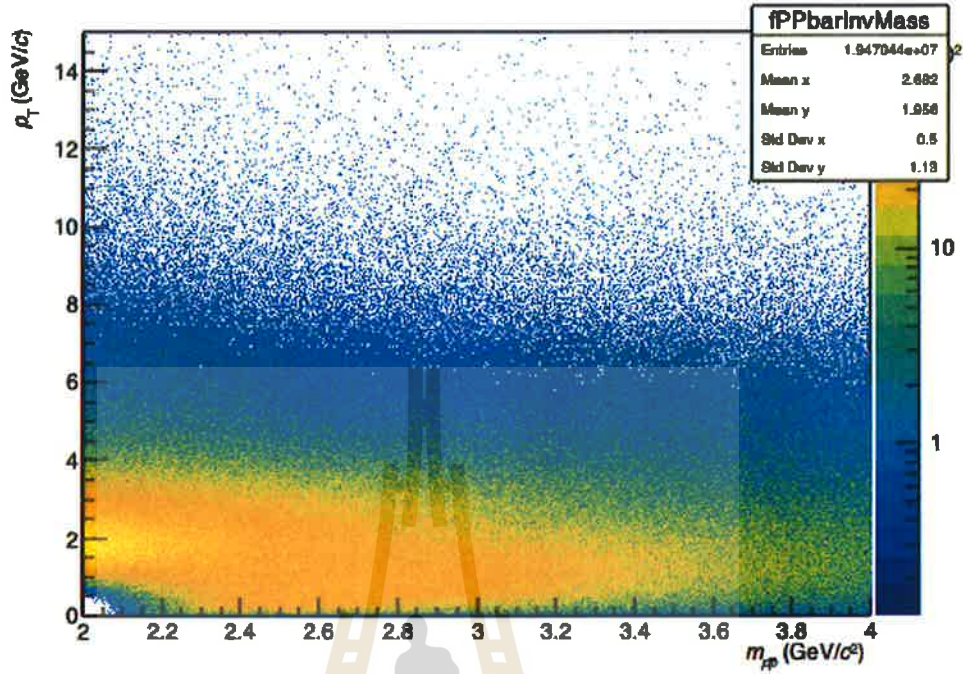


**Figure 4.15** The invariant mass spectrum of charmonium candidates reconstructing from proton-antiproton pairs versus its transverse momentum in the midrapidity  $|y| < 0.5$ .

called unlike-sign pair distribution. The unlike-sign pair distribution must contain the correlated pairs of signals, while like-sign pair do not contain any correlation of signal for the investigated charmed eta meson. Thus, the signal ( $S$ ) can be calculated by subtracting unlike-sign pair distribution ( $N^{+-}$ ) with like-sign pair distribution ( $N^{++}, N^{--}$ ) using the following equation:

$$S = N^{+-} - \sqrt{N^{++}N^{--}}, \quad (4.6)$$

#### 4.6.2 Event-mixing method

The combination of tracks in the same event must contain some fraction of the correlated pairs, while the tracks from different events mixed to describe the

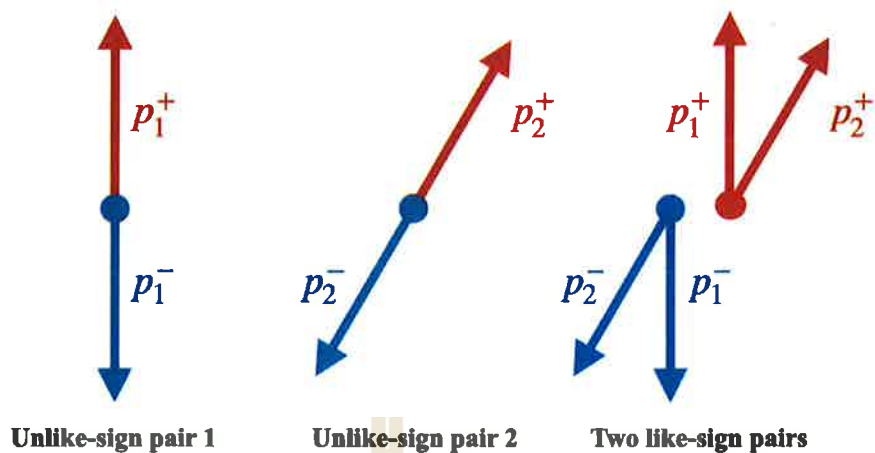


Figure 4.16 Sketch two like-sign pairs reconstructing from two unlike-sign pairs.

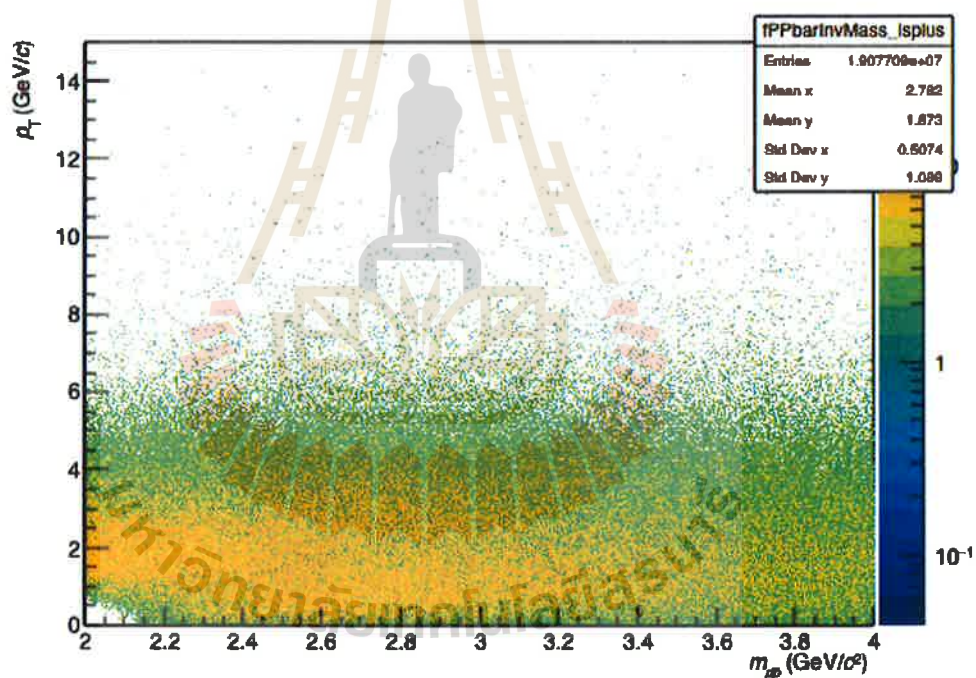
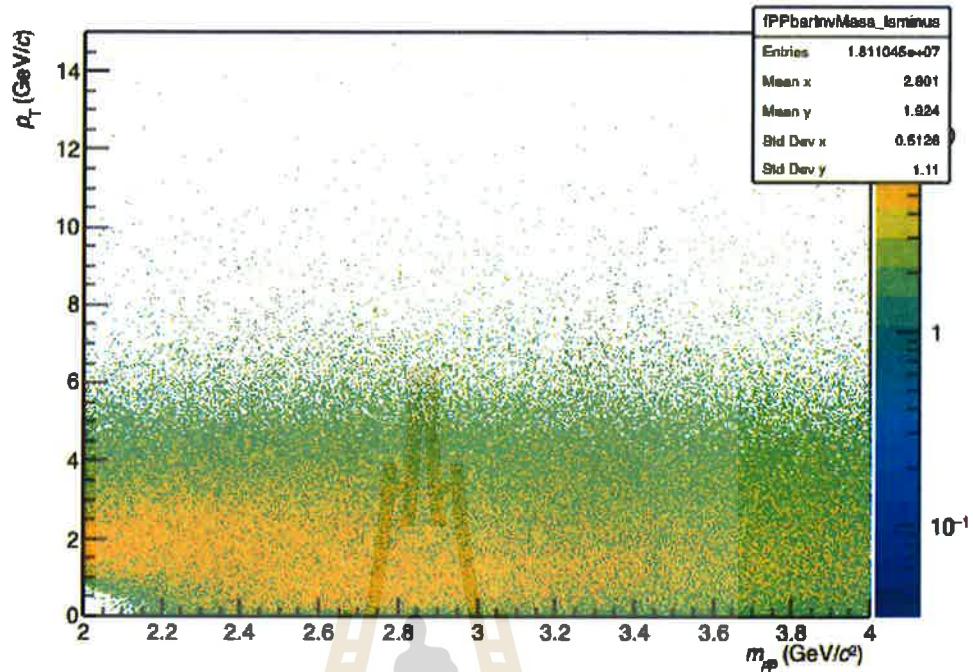


Figure 4.17 The positive like-sign pairs of charmonium candidates reconstructing from proton-proton pairs versus its transverse momentum in the midrapidity  $|y| < 0.5$ .

combinatorial background do not contain any correlated pairs. For example, in figure 4.19, the mixed event pair is reconstructed by using a positive track from



**Figure 4.18** The negative like-sign pairs of charmonium candidates reconstructing from antiproton-antiproton pairs versus its transverse momentum in the midrapidity  $|y| < 0.5$ .

event 1 and a negative track from event 2. Thus, the signal (S) can be calculated by subtracting the same event distribution (SE) with the mixed event distribution (ME). But the usage of this method needs some care, for instance because each collision event leads to different particle number of tracks in the detector. Therefore, the event mixing is only done for events with similar characteristics, e.g. only using events that have the same multiplicity.

### 4.6.3 Track rotational method

The correlation between daughter particles is kept in the 4-momentum vector, where the momentum of two daughters are equal in center-of-mass frame but point to different directions. Then, those daughters are Lorentz boosted via the

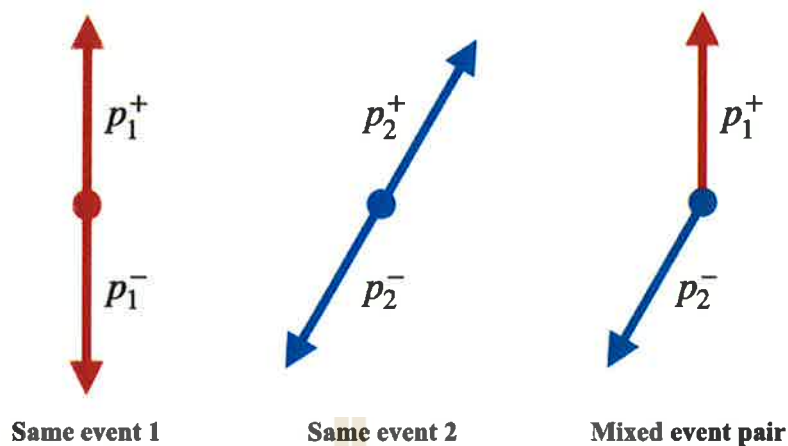


**Figure 4.19** Sketch of a mixed event pair by using positive charged particle from event 1 and negative charged particle from event 2.

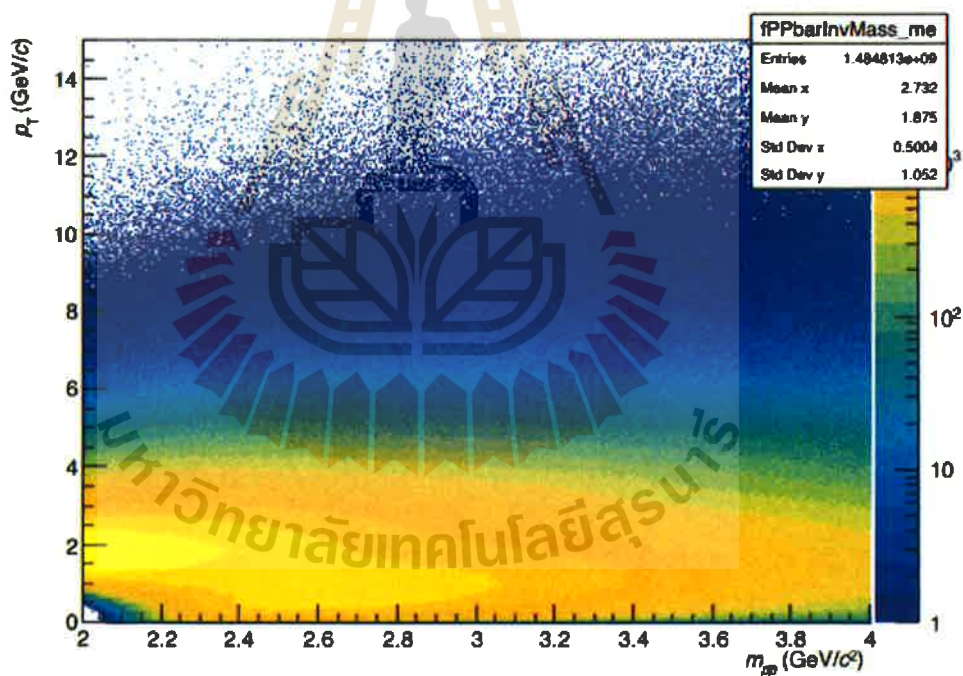


**Figure 4.20** The mixed event background of charmonium candidates reconstructing from proton-antiproton pairs versus its transverse momentum in the midrapidity  $|y| < 0.5$ .

momentum of mother. Therefore, the rotation of the momentum vector without changing the magnitude of one daughter can break the correlation of that pair. For example, in figure 4.21, the right sketch shows the 180-degree rotated positive track, which causes the reconstructed momentum of the mother to not point to the primary vertex and it becomes part of the uncorrelated background at the same time. In this method, we implement the algorithm to rotate the proton (antiproton) track by different angles in the range between  $5\pi/6$  and  $7\pi/6$  rad in azimuth (Adam et al., 2016), where the choosing angle can be anything but we select random angle around  $\pi$  rad for a better control over fluctuations and breaking more the correlation sufficiently than a smaller angle.

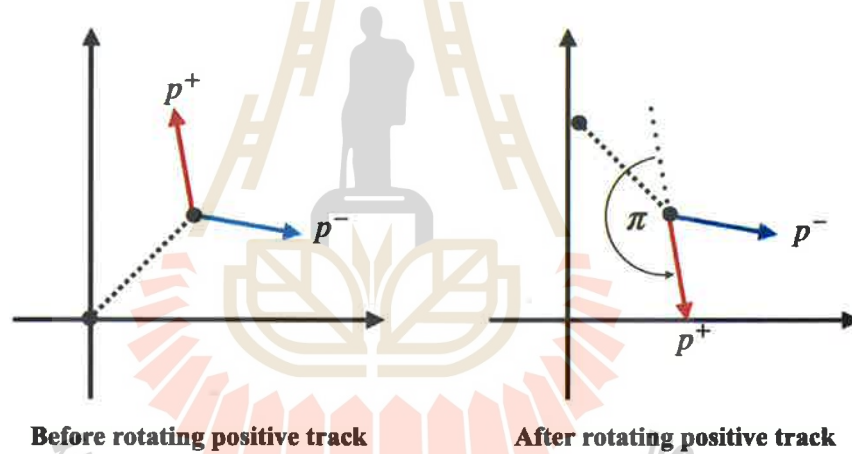


**Figure 4.21** Sketch of the momentum vector of positive and negative track, where the positive track is rotated. After breaking the correlation, the reconstructed momentum of the mother do not point to the primary vertex.

## 4.7 Background Subtraction

Before subtracting the background from the spectrum, we note that the estimated backgrounds from both track rotation and event mixing have higher statistics than the measured spectrum. Hence, these backgrounds are normalized

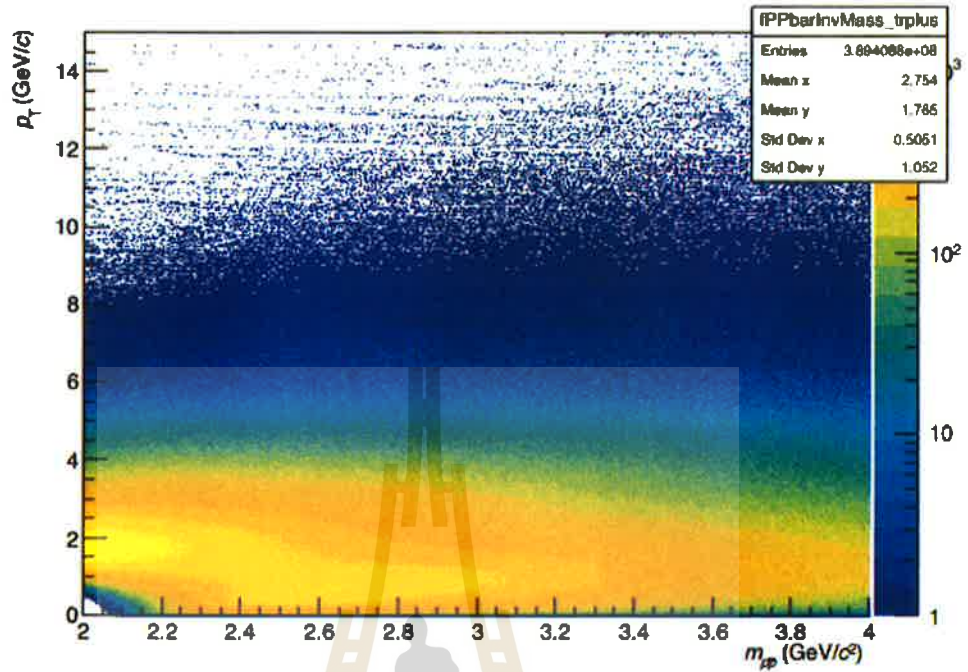


**Figure 4.22** The positive track rotational background of charmonium candidates reconstructing from rotated-proton and antiproton pairs versus its transverse momentum in the midrapidity  $|\eta| < 0.5$ .

to be the same shape as the background of spectrum and provide the distribution of signal higher than zero. In the case of background from like-sign pairs method, this backgrounds provides much lower statistics compared to the spectrum in the same momentum region, as shown in figure 4.24. The invariant mass spectrum of this figure is represented in different integrated transverse momentum regions,  $2 < p_T < 4$  GeV/c,  $4 < p_T < 6$  GeV/c,  $6 < p_T < 8$  GeV/c, and  $8 < p_T < 12$  GeV/c.

To normalize the estimated background, the background is scaled by the ratio of events in the spectrum's background over the events in the estimated background. The spectrum's background is determined by selecting the mass interval that is outside of the expected peak's region, the invariant mass of  $J/\psi$  is about  $3.096$  GeV/c<sup>2</sup>. Thus, we use the right-side of the spectrum in the range  $3.2$



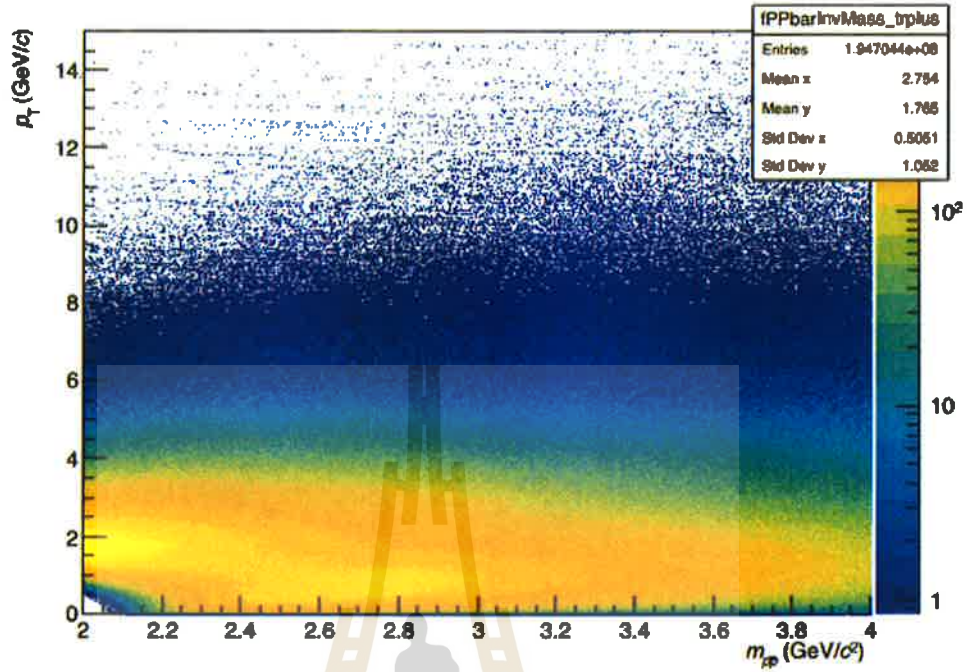


**Figure 4.23** The negative track rotational background of charmonium candidates reconstructing from proton and rotated-antiproton pairs versus its transverse momentum in the midrapidity  $|y| < 0.5$ .

-  $4.0 \text{ GeV}/c^2$  to normalize the estimated background. The normalized background ( $B'(m)$ ) is given by:

$$B'(m) = B(m) \frac{\int_{m_i}^{m_f} S(m') dm'}{\int_{m_i}^{m_f} B(m') dm'}, \quad (4.7)$$

where  $B(m)$  is the estimated background distribution,  $S(m)$  is spectrum of charmonium candidates,  $m_i$  and  $m_f$  are the selected minimum and maximum of the mass interval.

The results of normalizing the background for both event mixing and track rotation techniques are shown in the figure 4.24 and the results of using both estimated backgrounds are shown in figures 4.25 and 4.26 for event mixing and track rotation, respectively, where their distribution provided the similar distri-

bution shape. Considering the invariant mass after subtraction in each transverse momentum interval, there is only the invariant mass with integrated transverse momentum between  $6 < p_T < 8 \text{ GeV}/c$ , which shows a noticeable peak for both  $\eta_c$  and  $J/\psi$ , and both of them are found in both background subtraction methods. However, the subtraction leave a lot of residue background event which cannot reveal the distribution of signal, especially in lower momentum range that the most production yield sit at.

Nevertheless, due to the statistic of like-sign background being too low and high fluctuations, this method is no longer used for signal extraction in the next section.

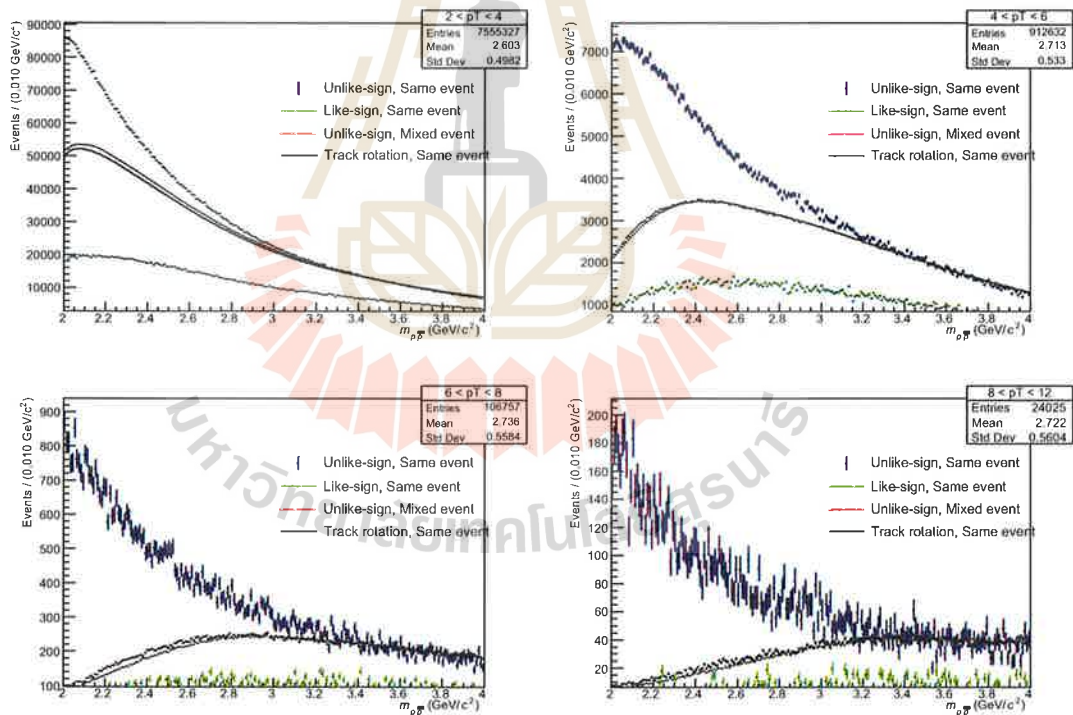


**Figure 4.24** Invariant mass spectrum of charmonium candidates with different integrated transverse momentum regions.

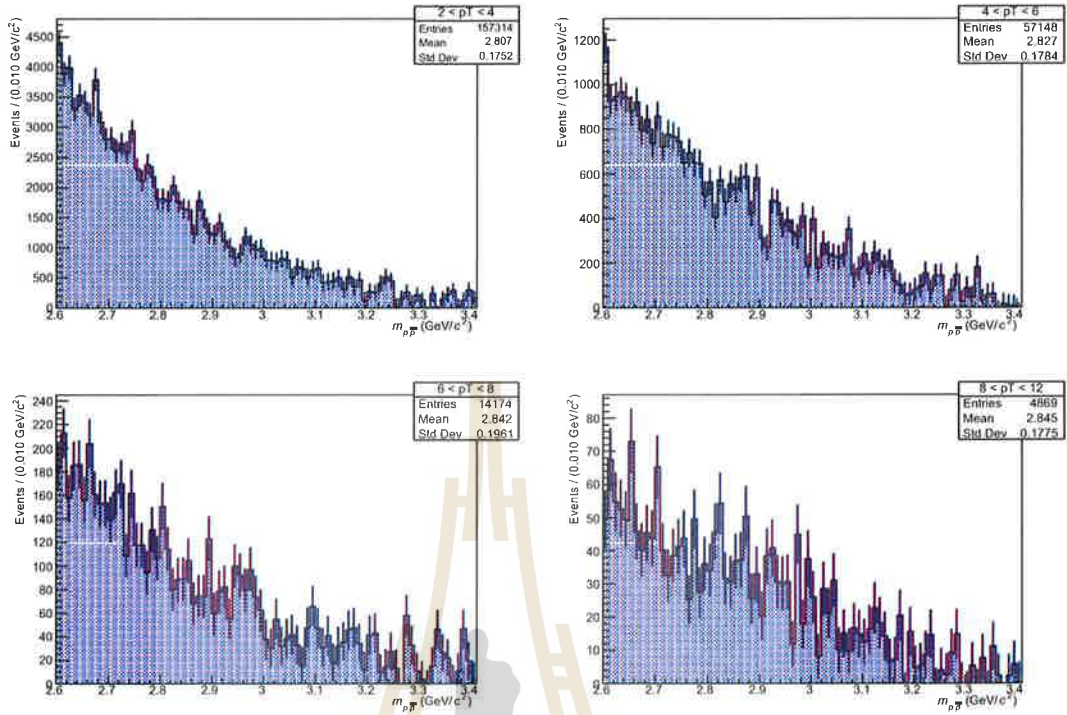


**Figure 4.25** Invariant mass spectrum after subtraction of mixed event background with different integrated transverse momentum regions.

## 4.8 Extraction of the signal

Usually, the signal distribution of short-lived particles is describe by Breit-Wigner function,

$$f(m) = \frac{Y}{2\pi} \frac{1}{(m - m_0)^2 + \Gamma^2/4}, \quad (4.8)$$

where  $m_0$  is the mass of initial particle,  $\Gamma$  is the Full Width at Half Maximum of the peak, which depends on the lifetime  $\tau$  via  $\Gamma = 1/\tau$ , and  $Y$  is the yield of events. However, in the cases where the signal line shape is dominated by smearing effects, it is often possible to model the signal peak with a Gaussian distribution, where the width  $\sigma$  is determined by the resolution of the mass measurement.

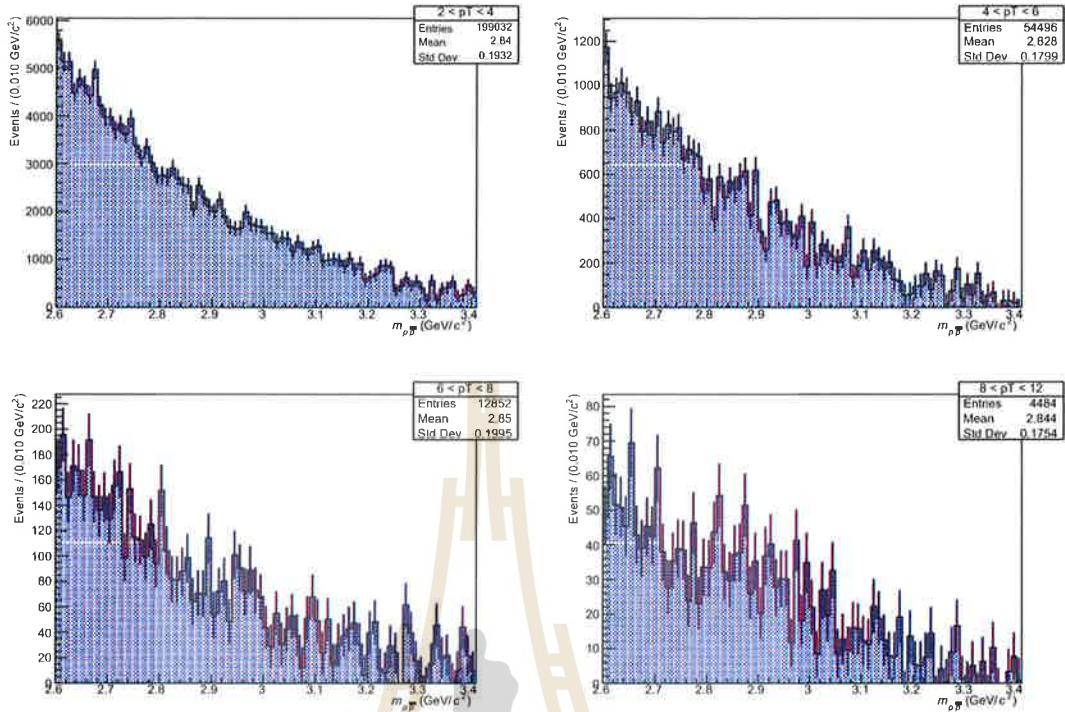


**Figure 4.26** Invariant mass spectrum after subtraction of track rotational background with different integrated transverse momentum regions.

The signal extraction is performed in two steps and is done utilizing the RooFit package (Kirkby and Verkerke, 2006). The first step fits the background distribution via both event mixing and track rotation methods in the sideband region of the invariant mass spectra by an exponential function. In the second step the signal is fitted with a double Gaussian function and the full signal-plus-background distribution is then re-fit using a combined fit function. The combined fit function has the following form:

$$f(m) = c_0 e^{-\alpha m} + \frac{c_1}{\sqrt{2\pi}\sigma_1} e^{-\frac{(m+m_1)^2}{2\sigma_1^2}} + \frac{c_2}{\sqrt{2\pi}\sigma_2} e^{-\frac{(m+m_2)^2}{2\sigma_2^2}}, \quad (4.9)$$

where  $c_0$ ,  $c_1$  and  $c_2$  are normalization coefficients of the exponential and the double Gaussian function, and  $\sigma_i$  and  $m_i$  are the width and mean of the Gaussian signal function, where  $i$  indicates each signal peak, assuming that the first peak is

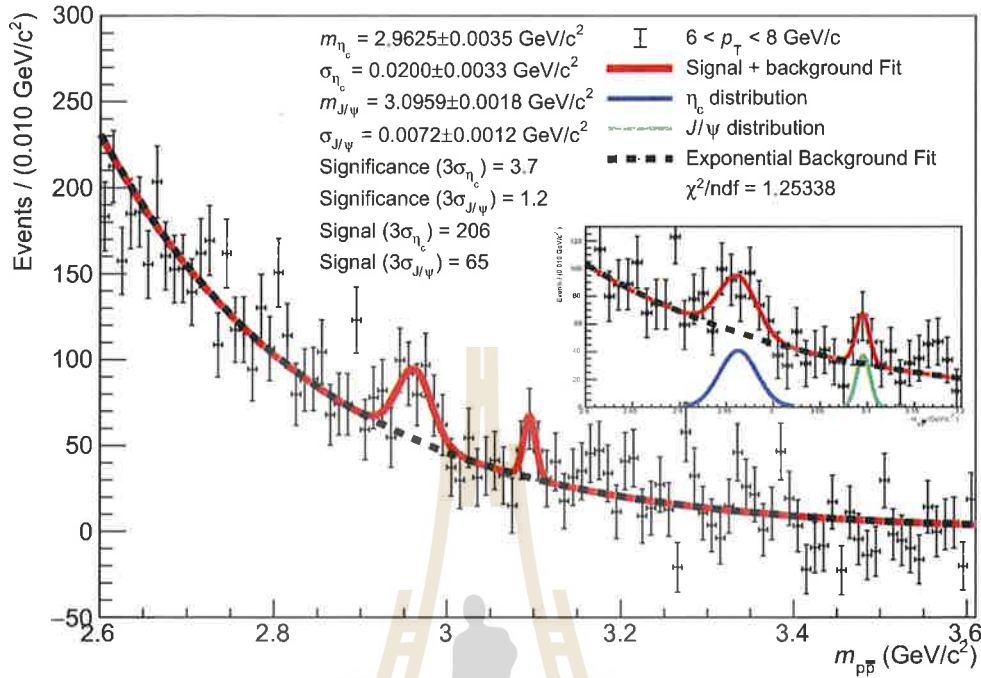
the  $\eta_c$  signal, and the second the  $J/\psi$  signal. The number of signals is determined as the integral of the Gaussian between  $\pm 3\sigma$ , and the background is determined as the integral of the background function in the same mass range.

Figure 4.27 and 4.28 show the fitting of  $\eta_c$  and  $J/\psi$  candidate invariant mass spectra subtracting background by event mixing and track rotation, respectively. The fit results are shown in Table 4.1. However, the fitting result show that the  $\eta_c$  are produced more than  $J/\psi$ , which conflicts to the table 2.2 that  $J/\psi$  provided the higher branching ratio to decay into proton-antiproton pair than  $\eta_c$  meson.

The significance of  $\eta_c$  and  $J/\psi$  signal are 3.7 and 1.2, respectively. However, for a goodness of signal peak, the significance of signal-over-background are required to be higher than 5 for reliable signal. Due to this analysis, we only found the peaks in the  $6 < p_T < 8$  GeV/c range, which requires more statistic to improve the significance.

**Table 4.1** The  $\eta_c$  and  $J/\psi$  fit results from the candidate invariant mass spectra subtracting background by event mixing and track rotation methods.

	Event Mixing	Track Rotation
$\eta_c$ Mass, GeV/c <sup>2</sup>	2.9625±0.0035	2.9635±0.0038
$J/\psi$ Mass, GeV/c <sup>2</sup>	3.0959±0.0018	3.0954±0.0016
$\eta_c$ $\sigma$ , GeV/c <sup>2</sup>	0.0200±0.0033	0.0217±0.0036
$J/\psi$ $\sigma$ , GeV/c <sup>2</sup>	0.0072±0.0012	0.0071±0.0010
exponential slope, $\alpha$	-4.0294±0.0665	-3.8661±0.0661
$\eta_c$ Signal( $3\sigma_{\eta_c}$ )	206	198
$J/\psi$ Signal( $3\sigma_{J/\psi}$ )	65	70
$\eta_c$ Significance( $3\sigma_{\eta_c}$ )	3.7	3.7
$J/\psi$ Significance( $3\sigma_{J/\psi}$ )	1.2	1.3



**Figure 4.27** Invariant mass spectrum after subtraction of the mixed event background.

## 4.9 Phase space simulation for two-body decays

To understand the behavior of the charmonium decay into proton-anti proton pair, the simulation will take a role to design the kinematic selection for those particle. In this work we use PYTHIA, the event generator for the charmonium production in proton-proton collisions at  $\sqrt{s} = 13 \text{ GeV}$ .

PYTHIA (Sjöstrand et al., 2015) is a program for simulating collisions of elementary particles and their evolution from few-body hard-scattering processes to a complex multi-particle system in the final state. In this work, we use PYTHIA8 together with ROOT (Brun and Rademakers, 1997), the data analysis framework, to analyze charmonium from the hard-scattering process of proton-proton collisions of a center-of-mass energy of 13 TeV. Due to the low probability of  $\eta_c$  and

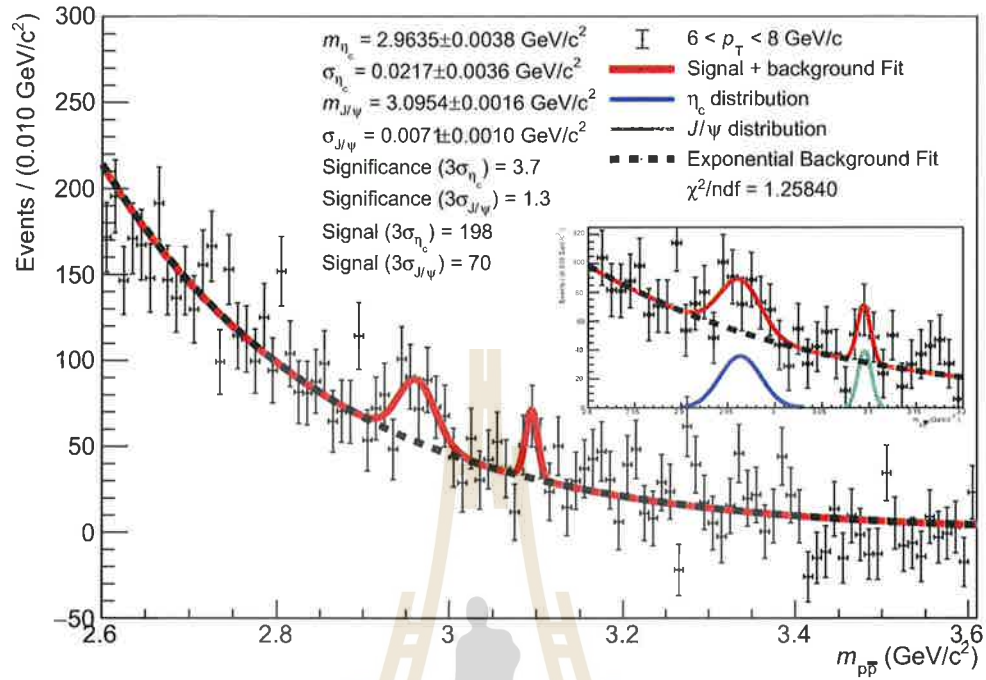


**Figure 4.28** Invariant mass spectrum after subtraction of the track rotational background.

$J/\psi$  decaying into proton and antiproton and the relatively low implemented production cross section in the simulation of minimum bias proton-proton collisions in PYTHIA, the configuration of PYTHIA was modified to produce only charmonium in these collisions and the decay mode was forced to be  $\eta_c, J/\psi \rightarrow p\bar{p}$  exclusively to increase the available statistics. This simulation also provide the invariant mass spectra with applying three reproducing background techniques to find the best best method to subtract the combinatorial background, the results are shown figure 4.29. Before the background subtraction, we clearly see that the track rotation method estimates the distribution very close to the shape of the signal, while the other two left the residue background after subtraction. Track rotation method also provides the highest significance. Considering the combination of two particles that used for constructing distribution, track rotation are

combination of protons and antiprotons that came from the same production as the signal distribution, while the like-sign pair and event-mixing methods are not the same.

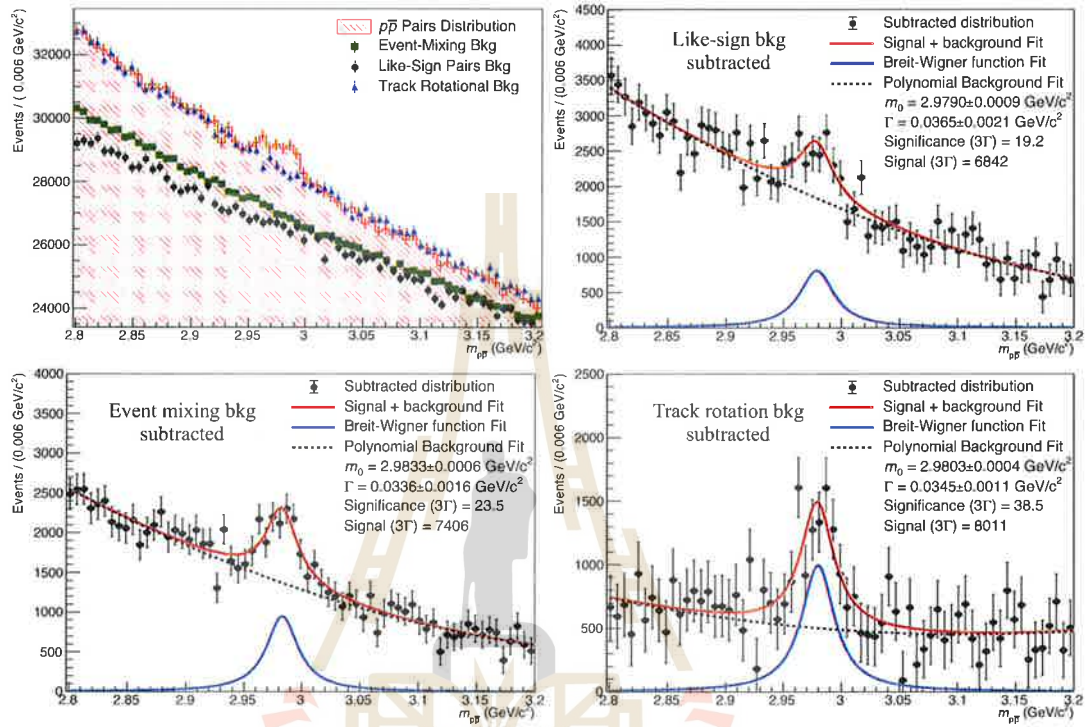


**Figure 4.29** Invariant mass distribution of  $\eta_c \rightarrow p\bar{p}$  candidates in the simulation of proton-proton collisions at  $\sqrt{s}=13$  TeV. The top-left panel displays the invariant mass distribution of all unlike-sign pairs together with the background distribution estimated with the like-sign pair, event mixing, and track rotation methods. The top-left and both bottom panels show the invariant mass distribution with fit function after background subtraction from the like-sign pair, event mixing, track rotation method, respectively.



# CHAPTER V

## CONCLUSION

This thesis has presented a measurement of two lowest-state of charmonium, charmed eta meson ( $\eta_c$ ) and  $J/\psi$  in  $pp$  collision at  $\sqrt{s} = 13$  TeV with ALICE at the LHC. The selected decay mode of these particle is  $\eta_c, J/\psi \rightarrow p\bar{p}$  because this is hadronic decay which most of charmonium-like particles can decay into this mode, as shown in the table 2.2, and it is relatively clean decay channel, with an expected high resolution efficiency and a huge amount of data from proton-proton collision.

The data have been taken from AliEn via using AliRoot and AliPhysics where we focus on the data of the charge hadron in central barrel tracking detector from Run2 experiment (2016-2018 periods). To retrieve the data, we implemented the AliAnalysisCODEX class from AliPhysics to reduce size of the ESDs data for collectable data.

In the chapter IV, we have implemented the analysis algorithms to work with the ALICE data. In the selection criteria, the track of protons and antiprotons are classified by the event and track selection which is using default parameters in analysis of ALICE data as shown in section 4.3 and 4.4. The particle identification of protons and antiprotons also performed by squared mass of particle in TOF, where the signals of proton and antiproton have been selected in the squared mass between 0.7 - 1.1 GeV/c<sup>2</sup>. Then the protons/antiprotons are identified by using the number of sigma cut in TPC and TOF, where the value of  $n\sigma_{TPC}$  and  $n\sigma_{TOF}$  cuts are given by 2 and 5, respectively.

The charmonium candidates are reconstructed from all possible combina-

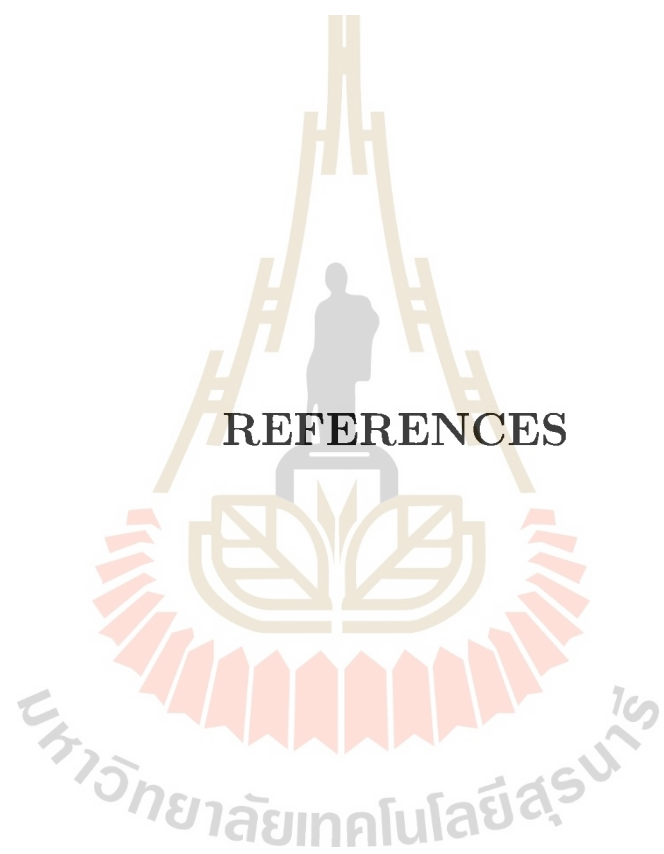
tion of protons and antiprotons using invariant mass reconstruction. However, some candidates are combinations of uncorrelated pairs, also known as combinatorial background. To subtract this background there are three techniques to reproduce the shape of background. First, the like-sign pairs is method to reproduce the background by combining the same charged particle which do not contain distribution of the targeted signal. Second, the event mixing reproduces background by combining tracks from different events. The last method, the track rotation, this method rotate one of the tracks before combining in between  $5\pi/6$  and  $7\pi/6$  azimuthal angle. However, the like-sign pairs method do not provide enough statistic to subtract the background from the spectra, so we design to drop this method.

The invariant mass spectra are separate in four different transverse momentum regions. After subtracting the spectra by event mixing and track rotation, there is only one region that appears the signal peaks of  $\eta_c$  and  $J/\psi$ . Usually, the signal of short-lived particle is described by Breit-Wigner function, but the signals in the result is dominated by smearing effect. Thus, the Gaussian function is used for fitting the signals, where mean and standard deviation of function represent mass of the particle and resolution of mass measurement.

The fitting results show mass of  $\eta_c$  and  $J/\psi$  are  $2.9625 \pm 0.0035$  GeV/ $c^2$  and  $3.0959 \pm 0.0018$  GeV/ $c^2$ , respectively, with the significance 3.7 and 1.2, respectively, where both subtraction method provide similarly results. After comparison of the fitted results, our analysis provides the invariant masses of both charmonium closing the database for Particle Data Group (PDG). However the significance of both peaks are not high enough to guarantee this measurement. Therefore, the more statistics is required, and the selection criteria is also optimised for lower momentum charmonium, where most of them sit in.

Further work, we plan to separate the charmonium production from prompt and not-prompt production, measure the cross-section of  $\eta_c$  and  $J/\psi$  in pp collision at  $\sqrt{s} = 13$  TeV in a midrapidity region and also measure the branching fraction of  $\eta_c \rightarrow p\bar{p}$  and  $J/\psi \rightarrow p\bar{p}$ . However, this process requires the Monte Carlo simulation of pp collision in ALICE for measuring the exact number of both charmonium decay in this process.





**REFERENCES**

## REFERENCES

- Adam, J., Adamová, D., Aggarwal, M. M., Aglieri Rinella, G., Agnello, M., Agrawal, N., Ahammed, Z., Ahmad, S., Ahn, S. U., Aiola, S., Akindinov, A., Alam, S. N., Albuquerque, D. S. D., Aleksandrov, D., Alessandro, B., et al. (2016). D-meson production in p-pb collisions at  $\sqrt{s_{NN}} = 5.02$  tev and in p p collisions at  $\sqrt{s} = 7$  tev. **Physical Review C**. 94(5): 054908.
- ALICE Collaboration (2010). The ALICE OFFLINE Bible. [Online]. Available: <http://aliweb.cern.ch/secure/Offline/sites/aliweb.cern.ch/Offline/files/uploads/OfflineBible.pdf>.
- Alice Collaboration (2014). Performance of the alice experiment at the cern lhc. **International Journal of Modern Physics A**. 29(24): 1430044.
- ALICE collaboration (2015). First results of the ALICE detector performance at 13 TeV. [Online]. Available: <https://cds.cern.ch/record/2047855>.
- ALICE Collaboration (2019). Physics coordination. [Online]. Available: <http://alice-collaboration.web.cern.ch/PhysicsCoordination>.
- ALICE collaboration (2020). TOF beta vs momentum performance in pp at 13 tev (lh15f). [Online]. Available: <https://alice-figure.web.cern.ch/node/9564>.
- Alme, J., Andres, Y., Appelshäuser, H., Bablok, S., Bialas, N., Bolgen, R., Bonnes, U., Bramm, R., Braun-Munzinger, P., Campagnolo, R., Christiansen, P., Dobrin, A., Engster, C., Fehlker, D., Foka, Y., et al. (2010). The ALICE TPC, a large 3-dimensional tracking device with fast readout for

ultra-high multiplicity events. **Nuclear Instruments and Methods in Physics Research Section A: Accelerators, Spectrometers, Detectors and Associated Equipment**. 622(1): 316–367.

Aubert, B., Barate, R., Boutigny, D., Gaillard, J.-M., Hicheur, A., Karyotakis, Y., Lees, J.-P., Robbe, P., Tisserand, V., Zghiche, A., Palano, A., Pompili, A., Chen, J.-c., Qi, N.-D., Rong, G., et al. (2003). Observation of a narrow meson decaying to  $D_s^+\pi^0$  at a mass of 2.32-GeV/ $c^2$ . **Physical Review Letters**. 90: 242001.

Aubert, J. J., Becker, U., Biggs, P. J., Burger, J., Chen, M., Everhart, G., Goldhagen, P., Leong, J., McCorrison, T., Rhoades, T. G., Rohde, M., Ting, S. C. C., Wu, S. L., and Lee, Y. Y. (1974). Experimental observation of a heavy particle  $J$ . **Physical Review Letters**. 33: 1404–1406.

Besson, D., Anderson, S., Frolov, V., Gong, D., Kubota, Y., Li, S., Poling, R., Smith, A., Stepaniak, C., Urheim, J., Metreveli, Z., Seth, K. K., Tomaradze, A., Zweber, P. K., Arms, K. E., et al. (2003). Observation of a narrow resonance of mass 2.46 gev/ $c^2$  decaying to  $D_s^{*+}\pi^0$  and confirmation of the  $D_{s,J}^*(2317)$  state. **Physical Review D**. 68(3): 032002.

Blum, W., Riegler, W., and Rolandi, L. (2008). *Particle detection with drift chambers*. Springer Science & Business Media.

Brun, R. and Rademakers, F. (1997). Root—an object oriented data analysis framework. **Nuclear Instruments and Methods in Physics Research Section A: Accelerators, Spectrometers, Detectors and Associated Equipment**. 389(1-2): 81–86.

CERN Accelerating science (2011). AliRoot documentation | ALICE offline.

[Online]. Available: <http://alice-offline.web.cern.ch/AliRoot/Manual.html>.

CERN Collaboration (2014). Root a data analysis framework | root a data analysis framework. [Online]. Available: <https://root.cern.ch/>.

Kirkby, D. and Verkerke, W. (2006). Home Page of the RooFit Toolkit for Data Modeling. [Online]. Available: <http://roofit.sourceforge.net/>.

Michel, G. (2020). R2E-EPC. [Online]. Available: [http://te-epc-lpc.web.cern.ch/te-epc-lpc/context/radiations/r2e\\_environment.stm](http://te-epc-lpc.web.cern.ch/te-epc-lpc/context/radiations/r2e_environment.stm).

Mikami, Y., Abe, K., Abe, T., Aihara, H., Akemoto, M., Asano, Y., Aso, T., Aushev, T., Bahinipati, S., Bakich, A., Ban, Y., Bay, A., Bizjak, I., Bondar, A. E., and Bozek, A. o. (2004). Measurements of the  $d_{sJ}$  resonance properties. **Physical Review Letters**. 92(1): 012002.

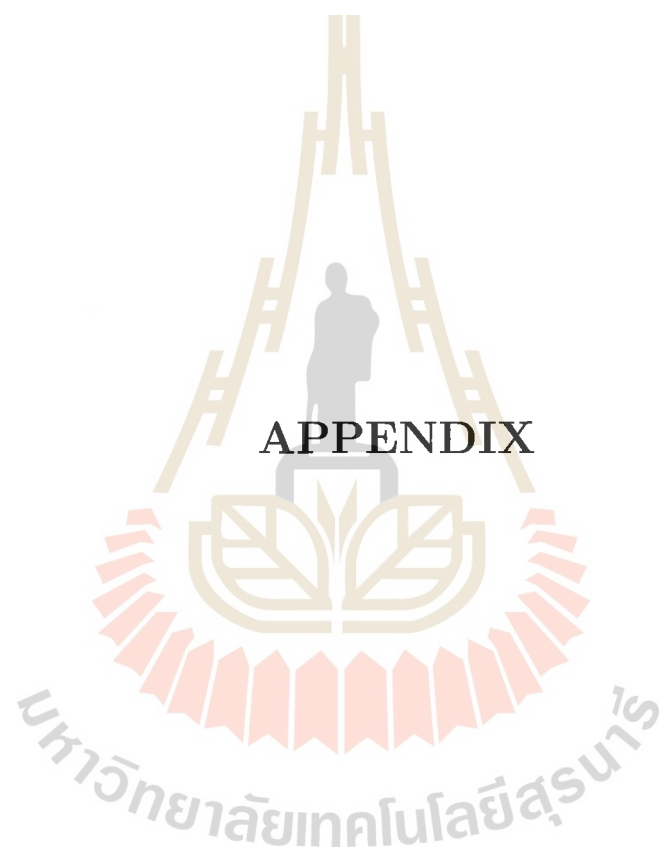
Particle Data Group, Zyla, P. A., Barnett, R. M., Beringer, J., Dahl, O., Dwyer, D. A., Groom, D. E., Lin, C. J., Lugovsky, K. S., Pianori, E., Robinson, D. J., Wohl, C. G., Yao, W. M., Agashe, K., Aielli, G., et al. (2020). Review of particle physics. **Progress of Theoretical and Experimental Physics**. 2020(8): 083C01.

Sjöstrand, T., Ask, S., Christiansen, J. R., Corke, R., Desai, N., Ilten, P., Mrenna, S., Prestel, S., Rasmussen, C. O., and Skands, P. Z. (2015). An introduction to pythia 8.2. **Computer physics communications**. 191: 159–177.

Tanabashi, M., Hagiwara, K., Hikasa, K., Nakamura, K., Sumino, Y., Takahashi, F., Tanaka, J., Agashe, K., Aielli, G., Amsler, C., Antonelli, M., Asner,

- D. M., Baer, H., Banerjee, S., Barnett, R. M., et al. (2018). Review of particle physics. **Physical Review D**. 98(3): 030001.
- Tauro, A. (2017). ALICE schematics. [Online]. Available: <https://cds.cern.ch/record/2263642?ln=en>.
- Teklishyn, M. (2014). *Measurement of the  $\eta_c(1S)$  production cross-section via the decay  $\eta_c$  to proton-antiproton final state.* (doctoral dissertation), Université Paris Sud - Paris XI.
- The ALICE Collaboration, Aamodt, K., Quintana, A. A., Achenbach, R., Acounis, S., Adamová, D., Adler, C., Aggarwal, M., Agnese, F., Rinella, G. A., Ahammed, Z., Ahmad, A., Ahmad, N., Ahmad, S., Akhmediev, A., Akhmediev, P., et al. (2008). The ALICE experiment at the CERN LHC. **Journal of Instrumentation**. 3(08): S08002.
- Voloshin, M. B. (2008). Charmonium. **Progress in Particle and Nuclear Physics**. 61(2): 455–511.





**APPENDIX**

# APPENDIX

## CENTRAL BARREL TRACKING FOR HADRON RUNLISTS

The ALICE collaboration provided countless data of particle collisions that were taken for several years and stored them into ALICE GRID. In this work, we focus on using the data proton-proton collisions with  $\sqrt{s} = 13$  TeV in central barrel tracking, which they were collected in 2015 until long shutdown of the LHC in 2019. We retrieved 2016 - 2018 data from ALICE GRID and the list of periods and good run numbers as shown in the table 1, 2 and 3 for the data in 2016, 2017, and 2018, respectively, where the runs represent the event reconstruction of the signals form central barrel tracking. The list of good run numbers were taken from ALICE data preparation group.

มหาวิทยาลัยเทคโนโลยีสุรนารี

**Table 1** The list of periods and good run numbers of proton-proton collisions with  $\sqrt{s} = 13$  TeV in central barrel tracking in 2016.

Period	Collision System	Centre-of-mass energy	Number of runlists
LHC16d	pp	13 TeV	18 runs
LHC16e	pp	13 TeV	11 runs
LHC16g	pp	13 TeV	17 runs
LHC16h	pp	13 TeV	67 runs
LHC16i	pp	13 TeV	14 runs
LHC16j	pp	13 TeV	34 runs
LHC16k	pp	13 TeV	165 runs
LHC16l	pp	13 TeV	58 runs
LHC16o	pp	13 TeV	71 runs
LHC16p	pp	13 TeV	42 runs

**Table 2** The list of periods and number of runlists of proton-proton collisions with  $\sqrt{s} = 13$  TeV in central barrel tracking in 2017.

Period	Collision System	Centre-of-mass energy	Number of runlists
LHC17c	pp	13 TeV	5 runs
LHC17e	pp	13 TeV	5 runs
LHC17f	pp	13 TeV	5 runs
LHC17g	pp	13 TeV	31 runs
LHC17h	pp	13 TeV	88 runs
LHC17i	pp	13 TeV	52 runs
LHC17j	pp	13 TeV	10 runs
LHC17k	pp	13 TeV	105 runs
LHC17l	pp	13 TeV	127 runs
LHC17m	pp	13 TeV	108 runs
LHC17o	pp	13 TeV	148 runs
LHC17r	pp	13 TeV	28 runs

**Table 3** The list of periods and number of runlists of proton-proton collisions with  $\sqrt{s} = 13$  TeV in central barrel tracking in 2018.

Period	Collision System	Centre-of-mass energy	Number of runlists
LHC18b	pp	13 TeV	25 runs
LHC18c	pp	13 TeV	49 runs
LHC18d	pp	13 TeV	44 runs
LHC18e	pp	13 TeV	41 runs
LHC18f	pp	13 TeV	59 runs
LHC18g	pp	13 TeV	11 runs
LHC18h	pp	13 TeV	2 runs
LHC18i	pp	13 TeV	9 runs
LHC18j	pp	13 TeV	1 run
LHC18k	pp	13 TeV	12 runs
LHC18l	pp	13 TeV	76 runs
LHC18m	pp	13 TeV	242 runs
LHC18n	pp	13 TeV	2 runs
LHC18o	pp	13 TeV	35 runs
LHC18p	pp	13 TeV	73 runs

# CURRICULUM VITAE

**NAME:** TAWANCHAT

**GENDER:** Male

SIMANTATHAMMAKUL

**NATIONALITY:** Thai

**DATE OF BIRTH:** NOVEMBER 13, 1994

**E-MAIL:** tawanchut1311@gmail.com

## EDUCATIONS:

- 2008 - 2013, High school at Ratchasima Wittayalai school.
- 2013 - 2016, Bachelor of Science, Physics department, Institute of science, Suranaree University of Technology/
- 2016 - 2020, Master of Science, School of Physics, Institute of Science, Suranaree University of Technology

## PUBLICATIONS

1. Nasawasd, T., Simantathammakul, T., Herold, C., Stockmanns, T., Ritman, J., Kobdaj, C. (2018). Track propagation methods for the correlation of charged tracks with clusters in the calorimeter of the  $\bar{P}$ ANDA experiment. **Journal of Instrumentation**, 13(02): T02008.
2. Simantathammakul, T. Dönigus, D. Herold, C. Kobdaj, C. (2020). Estimation of Combinatorial Background of  $\eta_c \rightarrow p\bar{p}$  in Proton-Proton Collisions at  $\sqrt{s}=13$  TeV, SUT-IVCST 2020.